Effects of Aqueous Organo-Sulfur Chemistry on Particulate MS-to-NSS Ratios in the Marine Atmosphere

Lei Zhu[1,4,5], *Athanasios Nenes [1,2], Paul H. Wine[1,3], J. Michael Nicovich[3]

[1]School of Earth and Atmospheric Sciences, GA Institute of Technology, Atlanta, GA
[2]School of Chemical and Biomolecular Engineering, GA Institute of Technology, Atlanta, GA
[3]School of Chemistry and Biochemistry, GA Institute of Technology, Atlanta, GA
[4]National Oceanic and Atmospheric Administration, Boulder, CO
[5]The Cooperative Institute for Research in Environmental Sciences, University of Colorado, Boulder, CO

Submitted to J. Geophys. Res., June 2005

Revised, October 2005

Keywords: DMS oxidation, aqueous phase chemistry, organo-sulfur compounds, MS-to-NSS ratio, cloud modeling, marine aerosol

Abbreviated Title: Effects of Aqueous Chemistry on MS/NSS ratios

*** Corresponding author email:** nenes@eas.gatech.edu

ABSTRACT

The oxidation of Dimethyl Sulfide (CH_3SCH_3, DMS) in the atmosphere could influence climate by affecting cloud condensation nuclei (CCN) concentrations and cloud properties. This work focuses on elucidating the importance of DMS-cloud interactions, especially the poorly understood aqueous phase chemical transformations of DMS oxidation products. For this purpose, we incorporate an oxidation mechanism of atmospheric DMS and its products within the modeling framework of a Trajectory Ensemble Model (TEM). Both marine cumulus and stratocumulus clouds are considered. It is found that the aqueous phase reactions of sulfur compounds contribute >97% of MS (methanesulfonate, $CH_3(O)S(O)O^-$) and >80% of NSS (non-seasalt sulfate) production in particles, and that about 30% of total MS and NSS production is from the aqueous phase oxidation of the organo-sulfur compounds. The aqueous phase MSI (methanesulfinate, $CH_3S(O)O^-$) + Cl_2^- reaction is found to be more important than MSI + OH as an MS source. The MS + OH reaction could consume almost 20% of MS and produce about 8% of total NSS within 3 days under typical marine atmospheric conditions.

1. Introduction

Understanding the contribution of biogenic emissions to the global sulfur cycle and its effect in global climate has motivated extensive study of Dimethyl Sulfide (CH_3SCH_3, DMS) oxidation in the marine boundary layer (hereon referred to as MBL) [e.g., *Arsene, et al.*, 1999; *Bates, et al.*, 1987; *Boucher, et al.*, 2003; *Charlson, et al.*, 1987; *Davis, et al.*, 1998; *Pham, et al.*, 1995; *Urbanski and Wine*, 1999; *von Glasow and Crutzen*, 2004]. Methanesulfonate ($CH_3(O)S(O)O^-$, MS) and non-seasalt sulfate (NSS) are considered the most important non-volatile products from DMS oxidation. Temperature, photochemical conditions, atmospheric dynamics, relative humidity and cloudiness can affect the relative production of MS and NSS from DMS oxidation. The MS-to-NSS ratio (MS/NSS) measured in aerosols is very useful for understanding the global sulfur cycle. However, the detailed processes involved in the oxidation of atmospheric DMS and production of MS and NSS are still only partially understood.

Yin et al. [1990a; 1990b] were the first to develop a comprehensive atmospheric DMS oxidation mechanism; subsequent studies are largely based on their original reaction scheme [e.g., *Arsene, et al.*, 2002; *Benkovitz, et al.*, 1994; *Chen, et al.*, 2000; *Chin, et al.*, 2000a; *Cosme, et al.*, 2002; 1999; *Davis, et al.*, 1998; 2004; *Gondwe, et al.*, 2003; 2004; *Hertel, et al.*, 1994; *Koga and Tanaka*, 1993; *Kreidenweis, et al.*, 1991; *Pham, et al.*, 1995; *von Glasow and Crutzen*, 2004]. An evaluation and sensitivity analysis of several DMS mechanisms (from *Yin et al.*[1990a; 1990b], *Koga & Tanaka* [1993], *Hertel et al*. [1994], *Benkovitz et al*. [1994] and *Pham et al*. [1995]) has been published by *Capaldo* and *Pandis* [1997]. Comparing simulations with *in-situ* observations suggest that the production of SO_2, NSS and MS from DMS oxidation

does not significantly vary between chemical mechanisms. *Capaldo* and *Pandis* [1997] found that SO_2 and MS are primarily formed in the gas phase and NSS production is primarily from the heterogeneous oxidation of SO_2. However, the mechanisms assessed by *Capaldo* and *Pandis* [1997] did not include heterogeneous oxidation of water soluble organo-sulfur compounds, i.e., dimethylsulfoxide ($CH_3S(O)CH_3$, DMSO), dimethylsulfone ($CH_3S(O)_2CH_3$, DMSO2) and methanesulfinate ($CH_3(O)SO^-$, MSI), which later on were proposed to contribute significantly to MS and NSS production. *Davis et al*. [1999] postulated that over 99% of MS and 80% of NSS in aerosols originate from aqueous phase oxidation of DMSO and its intermediates. Studies from *Campologo et al*. [1999], *Sciare et al*. [2000], *Legrand et al*. [2001], *Cosme et al*. [2002] and *von Glasow & Crutzen* [2004] found that the uptake of DMSO into the droplet phase and its subsequent oxidation have to be considered to reproduce observations of gas phase DMSO and condensed phase MS.

Potentially important atmospheric aqueous phase oxidants include O_3, H_2O_2, HO_2, OH, SO_4^-, Cl, Cl_2^- and NO_3. Studies have found that O_3 and H_2O_2 are the oxidants that are primarily responsible for aqueous phase SO_2 oxidation [*Botha, et al.*, 1994; *Erickson, et al.*, 1977; *Hoffmann*, 1986; *Kreidenweis, et al.*, 2003 and references therein; *Lagrange, et al.*, 1994; *Nahir and Dawson*, 1987]. Two studies of the O_3 + DMS reaction [*Gershenzon, et al.*, 2001; *Lee and Zhou*, 1994] demonstrated that the simultaneous uptake of DMS and O_3 and the subsequent surface reaction might play an important role in DMS oxidation. However, for oxygenated organo-sulfur compounds, the most important oxidants in the aqueous phase appear to be radicals. Two studies of the O_3 + DMSO reaction have shown this reaction to be very slow [*Lee and Zhou*, 1994; *Pryor, et al.*, 1984] and one study of DMSO reactions with a series of hydroperoxides [*Amels, et al.*, 1997] also demonstrated that hydroperoxides do not play

significant roles in DMSO oxidation in the aqueous phase. While previous work suggests the importance of the OH radical as an oxidant for organo-sulfur compounds [e.g., *Bardouki, et al.*, 2002; *Milne, et al.*, 1989; *Sehested and Holcman*, 1996; *Veltwisch, et al.*, 1980], our recent kinetics studies demonstrate that SO_4^-, Cl and Cl_2^- radicals are also potentially important oxidants of DMSO and MSI [*Zhu, et al.*, 2003a; 2003b, 2005] in the aqueous phase. For the first time, the temperature-dependent kinetics of the oxidation of organic sulfur compounds by OH and SO_4^- were studied in our recent work [*Zhu, et al.*, 2003a; 2003b]. In the present work, we attempt to study the importance of oxidation of organo-sulfur compounds by OH, SO_4^-, Cl_2^-, and Cl for conditions typically found in the marine boundary layer (MBL). The chemical evolution of the organo-sulfur species is studied by employing a Trajectory Ensemble Model (TEM) [*Stevens, et al.*, 1996]. We emphasize the application of the aqueous phase kinetic data obtained from our recent studies [*Zhu, et al.*, 2003a; 2003b, 2005]. We focus on the contribution of aqueous phase reactions to MS and NSS production, the temperature dependence of MS/NSS ratios, and effects of cloud dynamics on DMS oxidation.

2. Model Description and Chemical Mechanism

2.1 Description of Cloud Dynamics

The Trajectory Ensemble Model (TEM) of *Stevens et al*. [1996] employs a Large Eddy Simulation (LES) of a cloud field to obtain a set of Lagrangian trajectories to capture the variability of thermodynamic properties and dynamics within the cloud field. A detailed description of the TEM methodology, as well as the LES used to obtain the trajectories for this study is given by *Stevens et al.* (1996). Each trajectory contains information that characterizes

the thermodynamic state of an air parcel (pressure p, potential temperature in moist air θ, and the total (i. e., liquid and vapor) water mass mixing ratio, w_t) as it is advected throughout the flow field. The time evolution of the parcel thermodynamic state is used to drive a parcel model, which in its turn computes the liquid water content, water vapor supersaturation, temperature and cloud condensation nuclei (CCN) activation and droplet growth in the parcel. The equations that describe the evolution of trajectory properties and water vapor supersaturation profiles have been described before by *Medina* and *Nenes* [2004], and will not be repeated here. Embedded within the parcel model are the chemical mechanisms presented in section 2.2. The solutions obtained from the trajectories are used to obtain horizontally-averaged vertical profiles of concentration of each species. The main advantage of using TEM is that it incorporates the complex dynamics of clouds within the computationally efficient framework of a parcel model. A thorough evaluation of TEM can be found in *Stevens et al*. (1996).

2.2 Chemical Mechanism and Initial/Boundary Conditions

The DMS oxidation mechanism used in our simulations includes 12 gas phase reactions, 16 aqueous phase reactions, 10 aqueous phase equilibia and mass transfer of 12 species between the gas and the aqueous phase. The reactions are depicted in Figure 1. Gas-phase oxidants include OH, NO_3, BrO, Cl, NO and HO_2. Aqueous phase oxidants are O_3, H_2O_2, OH, SO_4^-, Cl_2^-, and Cl. The oxidation of organo-sulfur species initiated by aqueous phase SO_4^-, Cl_2^-, and Cl is included in a model simulation of DMS oxidation for the first time.

The concentration for each parcel species is calculated from a mass balance,

$$\frac{d[\mathrm{X}]}{dt} = \sum_i \mathrm{P}_i - \sum_j k'_j[\mathrm{X}] + \mathrm{E}_F[\mathrm{X}] \pm \mathrm{V}_T([\mathrm{X}]_g - [\mathrm{X}]_{eq}) - \mathrm{V}_D[\mathrm{X}]_{aq} \qquad (1)$$

where [X] represents the concentration of species X, expressed as molecule cm^{-3} if in the gas phase and mol L^{-1} if in the aqueous phase. P_i is the production rate of species X from reaction i (molecule cm^{-3} s^{-1} for gas phase, or mol L^{-1} s^{-1} for aqueous phase species), k'_j is the pseudo-first order loss rate of X due to reaction j (s^{-1}), E_F is the parcel expansion rate due to the ambient pressure (P) change (s^{-1}):

$$E_F = \frac{dP}{P\ dt} \tag{2}$$

V_T is the mass transfer coefficient for species X between the gas and the droplet phase (s^{-1}):

$$V_T = \frac{D}{\frac{r^2}{3}\left[1 + \frac{D}{r\alpha}\sqrt{\frac{2\pi}{RT}M_X}\right]} \tag{3}$$

where D is the diffusivity of the gaseous species X in air (m^2 s^{-1}), r is the radius of the droplet phase (m), α is the mass accommodation coefficient of gaseous X onto the droplets, M_X is the molecular weight of X (kg mol^{-1}), R is the universal gas constant (J mol^{-1} K^{-1}), and T is the temperature (K). $[X]_g$ and $[X]_{aq}$ represent concentrations of species X in the gas and aqueous phases, respectively (molecule cm^{-3} and mol L^{-1}). $[X]_{eq}$ is the equilibrium concentration of X in the gas phase (molecule cm^{-3}). A negative sign for the heterogeneous mass transfer term in Equation (1) is applied for gas-phase species while a positive sign is applied for aqueous-phase compounds.

V_D is the first order loss rate of the aqueous phase species due to wet/dry deposition of particles (s^{-1}). For clouds considered in this work (Dp (diameter) ≥ 10 μm), their main removal

mechanism is gravitational settling [*Seinfeld and Pandis*, 1998]; therefore, we adopt a simple approach by considering the deposition velocity of the droplet throughout the simulating field:

$$V_D = 1/\tau \approx v_s/H \quad (4)$$

where τ is the lifetime of particles/droplets (s), v_s is the settling velocity of particles/droplets (cm s^{-1}) and H is the height of the simulation field (cm). Further details about the effect of particle deposition on simulated MS/NSS ratios are discussed in section 3.2.

The gas phase and aqueous phase reaction rate coefficients are provided in Tables 1 and 2, respectively. Aqueous phase equilibrium constants are provided in Table 3. Henry's Law constants and mass accommodation coefficients for all species partitioning between the gas and droplet phases are provided in Table 4.

To simplify the simulations, all radicals are assumed to be in steady-state with a constant concentration throughout a simulation, which normally lasts for less than one hour. Within this short period, the meteorological and photochemical conditions normally do not change enough to affect the mixing ratios of free radicals. Table 5 depicts the concentrations used in this work; we choose daily average values representative of the remote marine atmosphere obtained from field measurements and model studies (references in Table 5). DMS is also assumed to be at steady state, with a constant concentration throughout the simulation. Concentrations of all other sulfur compounds are zero at the beginning of simulation and change with time according to equation (1). All parcels are below the cloud at the beginning of the simulation; therefore, the initial amount of cloud liquid water is assumed to be zero. Temperature, pressure and liquid water content are obtained from the trajectories.

3. Simulations in this Study

3.1 Clouds Considered

Given the global importance and dynamic differences between marine cumulus and stratocumulus clouds, both are considered in our simulations. Stratocumulus clouds, because of the wide coverage and long lifetime, provide an ideal environment for aqueous phase oxidation of organo-sulfur compounds. Although shorter-lived, cumulus convection plays a pivotal role in long range transport of trace species by effectively "pumping" them to the upper troposphere.

We used trajectories from simulations of two stratocumulus clouds, one in a non-drizzling (hereon referred to as "ASTEX-1"), and one in a heavily–drizzling state (hereon referred to as"ASTEX-2"). The formation of both clouds were forced by conditions observed during the Atlantic Stratocumulus Transition Experiment [*Albrecht, et al.*, 1995]. 500 trajectories for both "ASTEX-1" and "ASTEX-2" clouds were used to cover one hour of simulation time (hereon referred to as "1 simulation cycle"). Trajectories from deep convection simulations were also used; the formation of these clouds was forced by soundings obtained during the NASA Cirrus Regional Study of Tropical Anvils and Cirrus Layers - Florida Area Cirrus Experiment (CRYSTAL-FACE) (*Miao-Ling Liu*, personal communication), and 61 convective trajectories covered 30 minutes of simulation time (hereon also referred to as "1 simulation cycle"). Output was saved every 2 s in the stratocumulus trajectories and every 180 s in the cumulus trajectories.

Figure 2 displays average liquid water content (LWC) profiles for the stratocumulus and cumulus clouds considered. Between the two stratocumulus clouds (Figure 2a), "ASTEX-2"

has a higher average LWC (0.6 g m^{-3}) and lower cloud base (200 m) than "ASTEX-1" (0.4 g m^{-3} and 400 m, respectively). The cumulus cloud (Figure 2b) has an average LWC of ~1.0 g m^{-3}, a cloud base of about 500 m and a vertical extent of about 1500 m. As expected, the average updraft velocities of the cumulus cloud (2 m s^{-1}) are much higher than that of the stratocumulus cloud (0.2 to 0.4 m s^{-1}). Both ASTEX-1 and ASTEX-2 are energetic enough to maintain droplets of about 80 μm in diameter, and droplet number concentrations are in the range 10-400 cm^{-3} [*Albrecht, et al.*, 1995; *Stevens, et al.*, 1996]. For the CRYSTAL-FACE clouds, observed droplet number concentrations vary in a wide range from 250 to 2300 cm^{-3} and the average droplet diameters are in the range 0.5 – 60 μm [*Conant, et al.*, 2004]. Stratocumulus clouds cover the whole simulation field (2.8×2.8 km^2) while cumulus clouds cover only part of it (~22% of 6.0×6.0 km^2); the stratocumulus clouds last for the whole simulation period while the cumulus clouds do not. Instead, the latter form and dissipate on the timescale of ~30 min.

Non-drizzling stratocumulus clouds are the most ubiquitous in the marine atmosphere; therefore, many simulations will focus on the "ASTEX-1" trajectory set. Analysis of trajectories in the "ASTEX-1" cloud field indicated that air parcels stay in cloud for about 30% of the simulation time; in the MBL, aerosols spend roughly 3 hours per day in clouds [*Katoshevski, et al.*, 1999]. Assuming that the aqueous phase radical chemistry is important only in the droplet phase during daytime, and the cloud dynamics do not vary considerably when undergoing photochemical oxidation, cycling 15 times through the trajectory set (1 hour/cycle) will represent 3 days of atmospheric processing. The average lifetime of aerosols in the MBL is approximately 6 days [e.g., *Pham, et al.*, 1995]. Since we consider only cloudy conditions (which would reduce aerosol lifetime because of increased wet deposition), it is reasonable to assume that the modeled MS and NSS after 15 simulation cycles of stratocumulus clouds

represent those observed in the atmosphere for the average aerosol lifetime. For the cumulus clouds considered, it is found that trajectories stay in cloud for about 23% of the simulation time; therefore, 40 simulation cycles (30 min/cycle) are necessary to cover 3 days of in cloud processing. During continuous simulations, the same initial trajectory and cloud profiles are used repeatedly for each cycle, i.e., all parcels are reset below the cloud area after one simulation cycle then undergo the next cycle for the same trajectory and cloud conditions. The radical and DMS concentrations are constant throughout the whole simulation while the concentrations of DMS oxidation products increase as the number of cycles increases.

3.2 Sensitivity studies

To focus exclusively on DMS chemistry, initial concentrations of SO_2 are always set to be zero, i.e., all MS and NSS in the system are produced solely from local DMS oxidation. A "primary scenario" (PS) is considered, in which the steady state concentration of DMS is set to a typical value of 100 ppt [*Seinfeld and Pandis*, 1998]; the concentration of radicals for the PS are presented in Table 5. All sensitivity studies are based on perturbations of the PS.

The effect of wet/dry deposition of particles in MS and NSS production was studied. Figure 3 compares the temporal evolution of in-cloud average MS, NSS and MS/NSS obtained from PS simulations as the particle deposition rate increases from 0 to 7.8×10^{-5} s^{-1}. From Equation (4), the lower limit of $V_D \sim 2.0 \times 10^{-6}$ s^{-1} used in the simulation is based on the average aerosol lifetime, i.e., 6 days [e.g., *Pham, et al.*, 1995], and the average deposition velocity of ~ 0.2 cm s^{-1} for 10 μm particles over the ocean area within a height of ~ 800 m. The upper limit of $V_D \sim 1.0 \times10^{-4}$ s^{-1} is determined from the average settling velocity (v_s) of ~ 10 cm s^{-1} for droplets with diameter of 80 μm [*Seinfeld and Pandis*, 1998] when H = 800 m, corresponding to

approximately a 10-minute lifetime. As expected, concentrations of MS and NSS both decrease with increasing particle deposition rate within the range that covers the typical conditions of deposition rate in the cloudy MBL. Whether deposition is included in our model or not, the MS/NSS ratio becomes almost constant with a value of ~ 0.35 after 15 simulation cycles (Figure 3c). Only under conditions of strong wet deposition do we see a minor effect on MS/NSS, on the order of 20%. As the focus of this work is to study effects of aqueous phase reactions on the MS/NSS ratio, which is not significantly affected by the assumed wet deposition rate under typical conditions in the MBL, the above simplified method used in considering the deposition effect is appropriate, and, the rest of our simulations will not include the deposition term in Equation (1) to reduce the number of degrees of freedom in our system.

The steady-state DMS and radical concentrations as well as the branching ratios for reactions having more than one channel are varied to study their influence on MS and NSS production, and a summary of the sensitivity study results is listed in Table 6. Both MS and NSS production vary proportionally with the DMS steady-state concentration; therefore, the MS/NSS ratio is independent of the DMS concentration employed in the simulation. However, it is found that the simulated MS/NSS ratio is very sensitive to the concentration of gas phase radicals. An average BrO concentration of 10^7 molecules cm^{-3} from several studies [*Sander and Crutzen*, 1996; *Vogt, et al.*, 1996; *von Glasow and Crutzen*, 2004] was adopted in PS. As the BrO concentration increases from 10^6 to 10^7 to 10^8 molecules cm^{-3}, MS/NSS increases from 0.13 to 0.35 to 1.70. This trend supports the assessment of *von Glasow & Crutzen* (2004), and suggests that BrO can strongly influence the yield of SO_2 from DMS as well as the MS/NSS ratio. The BrO + DMS reaction produces primarily DMSO, which is quite efficiently taken-up by particles/droplets; hence, this reaction can potentially impact the gas-aqueous phase

distribution of sulfur species. Concentrations of OH(g), NO_3(g) and Cl(g) also affect MS/NSS and the SO_2 yield, but to a much smaller extent than BrO(g): as the concentration of OH(g) increases from 10^5 to 10^7 molecules cm^{-3}, MS/NSS decreases from 0.55 to 0.16; for the same adjustment of NO_3(g) concentration, MS/NSS decreases from 0.39 to 0.18; and when Cl increases from 10^3 to 10^5 molecules cm^{-3}, MS/NSS decreases from 0.49 to 0.10. These results indicate that OH(g), NO_3(g) and Cl(g) all favor the production of NSS because the DMS reactions with these radicals proceed primarily (exclusively for NO_3) *via* the H−abstraction channel at ~300 K. Typical average radical concentrations in the MBL are used in our model for the PS. Given the large variations in radical speciation and concentration with location and altitude, our simulation results can be used only as an average assessment, and could deviate from some measurements under conditions quite different from those in our model. As an example, it has been proposed that the only important oxidant of DMS in the Antarctica area is the OH radical [*Arimoto, et al.*, 2001; *Davis, et al.*, 2004]. When OH is the only radical, with an average concentration of 10^6 molecule cm^{-3}, our simulated MS/NSS ratio is about 45% lower than the result from PS. For the aqueous phase chemistry, OH is found to be the only radical to noticeably affect simulated MS/NSS in the present model: as the concentration of OH increases from 6×10^{-14} to 6×10^{-12} M, MS/NSS decreases from 0.47 to 0.08.

The mechanism adopted in our simulations (listed in Tables 1 and 2) represents our best current understanding of DMS oxidation. However, the uncertainty in some product yields is an important potential source of errors in this study. The DMSO(g) yield from the gas phase DMS + OH addition channel is thought to be within the range 0.5 to 1.0 [*Atkinson, et al.*, 1997; *Hynes, et al.*, 1993; *Hynes, et al.*, 1986; *Turnipseed, et al.*, 1996; *Williams, et al.*, 2001]. Our simulations indicate that this yield uncertainty has a small impact on the simulated MS/NSS ratio,

i.e., less than 10%. CH_3S has been proposed to be an important intermediate [e.g. *Martinez, et al.*, 1999; 2000; *Turnipseed, et al.*, 1993; *Tyndall and Ravishankara*, 1989a; 1989b] in determining yields of gas phase SO_2, H_2SO_4 and MSA from DMS oxidation. There is evidence that CH_3S can be oxidized by NO_2, HO_2 and O_3 in the presence of O_2 and H_2O [*Martinez, et al.*, 1999; 2000; *Turnipseed, et al.*, 1993; *Tyndall and Ravishankara*, 1989a; 1989b], but details of the mechanism remain elusive. The first order rate constant for the CH_3S reaction (G9 in Table 1) is estimated based on the kinetics data available from the above-referenced studies and typical concentrations of NO_2, HO_2 and O_3 in the MBL. Branching ratios for SO_2 and H_2SO_4 production from the oxidation of CH_3S are our own speculation. Simulations indicate that the simulated MS/NSS ratio is not noticeably affected by the CH_3S first order loss rate and branching ratios of SO_2 and H_2SO_4. In our mechanism, DMSO(aq) and MSI(aq) are assumed to be converted to MSI(aq) and MS(aq), respectively, with unit yield based on literature mechanistic studies [*Bardouki, et al.*, 2002; *Reuvers, et al.*, 1973; *Scaduto*, 1995; *Sehested and Holcman*, 1996; *Veltwisch, et al.*, 1980]. When both conversion yields are decreased to 80%, the steady-state concentrations of DMSO and MSI increase by ~20%; while, the change in simulated MS/NSS is less than 2%.

Our simulations find that the initial DMS concentration does not affect the simulated MS/NSS; however, when the initial concentration of SO_2 changes from 0 to 60 ppt, the simulated MS/NSS ratio decreases by nearly 60%. Due to the increased uptake of SO_2 into droplets and subsequent dissociation of H_2SO_3 (E3 and E4 listed in Table 3), the pH of the droplet phase decreases as SO_2(g) level increases. Though the S(IV) to S(VI) oxidation rate (by O_3 and H_2O_2) is affected by the acidity of solutions [*Alexander, et al.*, 2005; *Chameides and Stelson*, 1992; *Kreidenweis, et al.*, 2003; *Sievering, et al.*, 2004], the oxidation of organo-sulfur compounds by

radicals is not evidently affected [*Zhu, et al.*, 2005]. However, the production of both SO_4^- and Cl_2^- are sensitive to the acidity of solutions, and SO_4^- generation depends on the concentration of S(IV) in the aqueous phase [*Herrmann, et al.*, 2000]. As the steady-state concentrations of SO_4^- and Cl_2^- both change by two orders of magnitude, the simulated MS and NSS production rates both change by less than 10%. Therefore, the MS and NSS production from aqueous phase oxidation of organo-sulfur compounds are not significantly affected by the acidity of solution or S(IV) concentrations.

4. Results

4.1 Stratocumulus Simulations

4.1.1 "Primary Scenario" (PS)

Figure 4 presents vertical profiles of DMSO(g), SO_2(g), MS(aq) and NSS(aq) generated from DMS oxidation, after 1, 5, 10 and 15 simulation cycles of the PS. The rapid heterogeneous mass transfer of DMSO and SO_2 is responsible for the characteristic "S" shape of the vertical concentration profiles of DMSO(g) and SO_2(g) (i.e., concentrations below the cloud area are higher than those within the cloud area). Because of the efficient uptake of DMSO into droplets and the fast oxidation of DMSO in both the gas and the aqueous phases, the steady-state concentration of DMSO is attained within 1-2 simulation cycles. Therefore, the concentration profiles of DMSO(g) after 1, 5, 10 and 15 simulation cycles are almost identical (Figure 4a). Relative to DMSO, SO_2 has a lower solubility and reactivity; it is thus expected that it will take a longer time for SO_2 to approach its steady-state concentration. Indeed, as can be seen in Figure 4b, about 10 simulation cycles are needed for SO_2(g) profiles to approach a steady state.

The MS concentration increases linearly with time (Figure 4c), but the NSS accumulation accelerates with time (Figure 4d). The different trend in MS and NSS production is mainly due to different sources of these two species; MS is primarily from the oxidation of aqueous phase organic sulfur species, while the oxidation of sulfur species and the uptake of gaseous H_2SO_4 contribute nonlinearly to NSS production. A detailed discussion on this topic follows in section 4.1.2. Different from DMSO and SO_2, concentrations of MS and NSS keep increasing within 15 simulation cycles. This is expected because the main sink for both MS and NSS is wet deposition (because of their low volatility and reactivity), which is excluded in the PS (see above).

4.1.2 Contribution of Aqueous Phase Reactions to MS and NSS Production

To quantify the contribution of heterogeneous processes to MS and NSS production as well as to the removal of SO_2(g) and DMSO(g), results are compared for four simulation scenarios including: *i*) only gas phase reactions to produce DMSO and SO_2 (GP), *ii*) all gas phase reactions (GA), *iii*) all gas phase reactions and mass transfer to the aqueous phase (GM), and, *iv*) all multi-phase physical and chemical transformations (PS). Clearly, scenarios GP and GM would never occur in the atmosphere; however, they could be employed to obtain some useful information. Production of SO_2 from the H−abstraction and addition channels of DMS oxidation (a major issue for atmospheric chemists) can be assessed by comparing scenarios GP and GA. Production of SO_2 under cloud-free and cloudy conditions can be compared from scenarios GA and PS and contributions of aqueous phase transformations to MS and NSS production can be evaluated by comparing MS and NSS production between scenario GM and PS.

Concentrations and product yields of SO_2(g), DMSO(g), MS and NSS after 15 simulation cycles of the above four scenarios are listed in Table 7. Relative to GP, the GA scenario has a 10% increase in the SO_2(g) yield, but a 20% decrease in the DMSO(g) yield, because DMSO is oxidized more rapidly than SO_2 by OH; in addition, SO_2 is the dominant gas phase end product from DMSO + OH. For the conditions considered in our simulations, the H−abstraction channel is the dominant pathway and accounts for about 85% of total SO_2 production, while the addition channel (through oxidation of DMSO) contributes about 15%. As discussed by *De Bruyn et al*. [2002], the SO_2(g) yield reported in the literature varies between 50% and 100%, depending on the DMS oxidation mechanism and simulation conditions employed. Our simulated SO_2(g) yield under cloud-free conditions (GA) falls within this range and agrees well with estimates from *Ayers et al*. [1997], *De Bruyn et al*. [1998], *Davis et al*. (1999), *Mari et al.* [1999], *Chin et al*. [2000b], and *Shon et al*. [2001].

Given the substantial solubility of DMSO in water, in the absence of an efficient aqueous sink (i.e., GM scenario) DMSO can be present in both gas and aqueous phases in significant amounts; hence, the concentration and yield of DMSO for GM increases compared to GA. The SO_2 concentration remains almost identical for GA and GM, but its fraction in the total sulfur products for GM decreases dramatically compared to GA (Table 7), suggesting that the mass transfer of SO_2 into the aqueous phase is balanced by SO_2 production from increasing gas phase DMSO oxidation for GM. For the PS, where both gas and aqueous phase transformations are considered, MS and NSS become dominant and contribute about 23% and 67%, respectively, to the total sulfur products. Meanwhile, the SO_2 yield in the PS becomes 8% because heterogeneous processes, i.e., uptake of DMSO, S(IV) and their subsequent aqueous phase

oxidation are much faster than gaseous SO_2 oxidation, and dominate over the slow production of SO_2(g).

Understanding the atmospheric fate of DMSO is central for quantifying the amount of sulfur species in the gas and condensed phases. Our simulations indicate that heterogeneous processes contribute roughly 90% to the DMSO sink, much higher than published estimates of ~50% [*Cosme, et al.*, 2002; *Davis, et al.*, 1998; *Legrand, et al.*, 2001; *Sciare, et al.*, 2000]. This suggests that aqueous phase transformations may be even more important for the sulfur cycle than previously thought. Meanwhile, uptake from the gas phase is the primary source of DMSO in the aqueous phase, as our simulations suggest that aqueous phase oxidation of DMS is a minor contributor (10-15%). Reported Henry's Law constants for DMSO vary over almost 4 orders of magnitude: 1400 from *Gmehling et al.* [1982] and *Betterton et al*. [1992], $> 5\times10^4$ from *De Bruyn et al*. [1994], 1×10^6 from *Lee* and *Zhou* [1994] and $\geq10^7$ from *Campolongo et al.* [1999] and *Legrand et al.* [2001], in units of M atm^{-1}. Our simulations demonstrate that MS production increases by about 15% while NSS production remains constant within this range. In order to maximize the effect of aqueous phase chemistry in DMS oxidation, we adopted the upper limit of the highly uncertain Henry's Law constant for DMSO. Despite the substantial uncertainty, its effect on MS production and MS/NSS is small, i.e., 15-20%; this indicates that the aqueous phase oxidation, not solubility, drives DMSO(g) into the aqueous phase. Of the four aqueous radicals studied, OH is the most efficient at scavenging DMSO and contributes ~55% to total aqueous DMSO loss. The DMSO + SO_4^- reaction accounts for ~34% of total aqueous DMSO loss, and Cl_2^- consumes another 10%. This ranking of radicals based on their importance in DMSO removal agrees well with estimates based on the rate coefficient of each

reaction [*Zhu, et al.*, 2003a; 2003b, 2005] and the steady-state radical concentrations listed in Table 5.

Comparing simulations of GM and PS indicates that uptake of gas-phase MSA accounts for ~3% of total MS production. This value is slightly higher than the estimates of ~1% from *Davis et al.* (1999) and 2% from *von Glasow* & *Crutzen* (2004). The difference between studies may be from the gas phase MSIA + OH reaction pathway which can generate MSA [with a yield of 0-10% from *Kukui, et al.*, 2003]. We adopted the upper limit (10%) in our simulations to maximize the effect of gas phase MSA production. If this yield is halved to 5% (a value used by *von Glasow* & *Crutzen* (2004)), the gas phase formation of MSA will account for <2% of total MS production. As shown in Figure 3c, the MS concentration increases almost linearly with time for PS, which also suggests that MS has one dominant source, i.e., aqueous phase production. *von Glasow* & *Crutzen* (2004) postulated that the MSI + OH reaction is the only important direct source of MS. In our simulations, the MSI + Cl_2^- reaction (not included in their studies) is found to be more important than MSI + OH and contribute ~ 65% of total MS production compared to ~ 25% for MSI + OH. The reactions MSI + SO_4^- and DMSO2 + OH account for < 10% of total MS production. This is an important new finding on the potential role of aqueous phase radicals other than OH in the atmospheric cycling of organo-sulfur compounds.

Our simulations suggest that gas phase production contributes ~9% of total NSS production. This value is in agreement with *von Glasow* & *Crutzen* (2004), but is 50% lower than the observational study of *Davis et al*. (1999). Incomplete knowledge of the DMS oxidation mechanism, SO_2 sources other than DMS, as well as different concentrations of DMS and radicals are likely responsible for this difference. In our study, oxidation of CH_3S and SO_2 are two sources of gas phase H_2SO_4. When the branching ratio of H_2SO_4 from CH_3S oxidation

is adjusted by a factor of 2 from the value listed in Table 1, the contribution of gas phase H_2SO_4 varies from 5% to ~17%, still a minor contributor to NSS production. Therefore, we conclude that the gas phase accounts for ≤3% of MS and 5-17% of NSS production.

In the PS simulation, DMS oxidation increases total non-seasalt mass by about 2.8 nmol m^{-3} with a MS/NSS ratio of ~0.35. When in-cloud aqueous phase reactions are excluded from the simulation (i.e., scenario GM), the MS/NSS ratio decreases to ~0.12, because aqueous phase reactions contribute more to MS than to NSS production. To estimate the contribution from the aqueous phase reactions of organo-sulfur species to the total mass growth, all these reactions are "turned off" (scenario NOS, listed in Table 7). Heterogeneous oxidation of S(IV) is found to be the most important source of the nonvolatile mass, contributing over 60% of total sulfur production. The aqueous phase oxidation of organo-sulfur compounds accounts for ~30% of total MS and NSS production, and the other 5-10% is due to mass transfer of gas phase MSA and H_2SO_4.

4.1.3 Temperature Dependence of MS and NSS Production

Assuming PS conditions, we explored the effect of temperature changes on the production of MS, NSS and their ratio; the results for the "ASTEX-1" stratocumulus cloud are depicted in Figure 5. MS production decreases with increasing temperature (Figure 5a) for two reasons: *i*) the production of gas phase DMSO from both sources (DMS + OH and DMS + BrO) decreases with increasing temperature, and, *ii*) DMSO becomes less soluble as temperature increases (Table 4); both of these effects result in a reduction in the aqueous DMSO concentration at high temperatures. The aqueous phase DMSO oxidation rate increases with temperature (Table 2), but it is limited by mass transfer of DMSO from the gas phase. Depleted

DMSO concentrations affect MS production by decreasing the amount of MSI (the most important precursor of MS). Thus, the temperature-dependence of MS production follows that of aqueous phase DMSO.

The temperature dependence of NSS production (Figure 5b) is not monotonic. In the first 3-4 cycles, NSS production always decreases with increasing temperature. For longer integration times, NSS reaches a maximum at 288 K. This behavior can be interpreted by linking NSS with its primary source, SO_2. As the main gas phase end product from DMS oxidation, the total SO_2 production rate increases with increasing temperature. The solubility of SO_2 in water however decreases with increasing temperature (Table 4), thus partitioning less SO_2 to the aqueous phase. As a result, SO_2 is accumulated in the gas phase at high temperatures. Finally, all aqueous phase reactions of S(IV) with O_3 and H_2O_2 have positive temperature dependences (Table 2). The opposing temperature dependence of SO_2 solubility and S(IV) oxidation yields a "transition point" for NSS production at each temperature. Before the "transition point", uptake of SO_2 is rate-limiting in NSS production and after that S(IV) oxidation become more important in determining the NSS production rate. The occurrence of the "transition point" depends on the time needed for SO_2 to achieve the steady state (2-3 simulation cycles at low temperatures and ~ 10 cycles at high temperatures; Figure 5b).

As MS and NSS production vary differently with temperature, the simulated MS/NSS exhibits a complex temperature dependence (Figure 5c). For all temperatures studied, MS/NSS ratios decrease with time and eventually approach a constant value representing the steady-state MS/NSS at each temperature. It takes longer for MS/NSS to reach steady state at higher temperatures than at lower temperatures because of decreased aqueous S(IV) concentrations at higher temperatures. For consistency, we compare MS/NSS ratios at steady state for all

temperatures considered. The highest MS/NSS with a value of ~ 0.75 is observed at 278 K after 15-20 cycles, and the lowest MS/NSS with a value of ~ 0.23 is observed at 318 K after 30-35 cycles.

The contribution of aqueous-phase transformations to the total production of MS and NSS also varies with temperature. Simulations suggest that aqueous phase chemistry contributes 99% and 95% to total MS production at 278K and 318K, respectively. This is not surprising, since total MS production decreases with increasing temperature (Figure 5a) while the gas-particle partitioning of MSA remains practically unchanged. Therefore, partitioning of MSA between the gas and aqueous phases contributes more to total MS production at higher temperatures than at lower temperatures. For the same reason, aqueous phase reactions contribute less than 80% to total NSS production at 318K and over 90% for temperatures lower than 300K.

von Glasow & Crutzen [2004] estimated that the MS + OH reaction could contribute 10% to total NSS production. In a recent kinetics study, *Zhu et al.* [2003a], reported a room temperature rate constant consistent with the value adopted by *von Glasow & Crutzen* [2004], which is the lowest of three previous literature values (1.3×10^7 by *Olson & Fessenden* [1992], 5.4×10^7 by *Milne et al.* [1989], and 1.4×10^9 by *Lind & Eriksen* [1975], in units of M^{-1} s^{-1}). For the first time, the temperature-dependent kinetics of this reaction have been reported by *Zhu et al.* [2003a]. The high activation energy of MS + OH, i.e., ~22 kJ mol^{-1}, makes this reaction potentially important in affecting the MS/NSS ratio at high temperatures. To quantify the contribution of MS + OH to NSS production and MS removal, we compared the results of MSA, NSS and MS/NSS obtained from the PS with those from the simulation without MS + OH under otherwise identical conditions. At 300 K, it is found that the MS + OH reaction consumes

almost 20% of MS and accounts for 8% of total NSS production; thereby, decreasing MS/NSS by ~25%. Our simulations indicate that the effect of the MS + OH reaction on MS/NSS ratios varies significantly with temperature: MS + OH scavenges 9% of MS and creates 8% of NSS at 278 K, while it can consume 27% of MS and produce 23% of NSS at 318 K; as a result, MS/NSS ratios decrease by 17% at 278 K and by 40% at 318 K due to MS + OH. These results indicate that even though the MS + OH rate constant is relatively slow, atmospheric aerosols reside in the MBL long enough for this reaction to significantly affect the MS/NSS ratio.

4.2 Comparison between trajectory sets

Comparing the simulations from different cloud trajectory sets provides useful insight on the main parameters controlling the organo-sulfur profiles and their temporal evolution. Figure 6 compares the temporal evolution of in-cloud average MS, NSS and MS/NSS for all cloud trajectory sets considered in this study. The simulations were carried out assuming PS conditions.

4.2.1 Comparison of "ASTEX-1" and "ASTEX-2" Simulations

It can be seen that MS production from two simulations are close (Figure 6a), while the NSS production from "ASTEX-2" is apparently faster than that from "ASTEX-1" (Figure 6b), due to different primary precursors of MS and NSS. The mass transfer of DMSO and its oxidation in the aqueous phase are fast enough in both clouds so that the gas-phase DMSO production is rate limiting for MS production; hence MS production is not noticeably affected by the striking differences between ASTEX-1 and ASTEX-2. On the other hand, NSS production is evidently higher for "ASTEX-2" than "ASTEX-1" simulation because of the higher LWC available for SO_2 uptake in the "ASTEX-2" cloud. As a result, MS/NSS for the

"ASTEX-2" cloud is about 40% lower than the "ASTEX-1" cloud after 15 simulation cycles.

4.2.2 Comparison of Cumulus and Stratocumulus Simulations

Compared to stratocumulus clouds, cumulus clouds generally have a smaller spatial extent and shorter lifetime. This will have a profound effect on MS production and MS/NSS. Since cumulus convection is a primary mode of introducing NSS into the free troposphere, this may give insight to MS/NSS observed in the free troposphere.

Only 14 out of 61 total trajectories in the cumulus cloud field considered in this work go through the cloud and affect DMS oxidation through in-cloud chemistry. Two trajectory sets are considered: "CF-All" contains all 61 trajectories in the cloud field; "CF-Cloud" contains only the 14 trajectories that pass through the cloud area. Analysis of trajectories in the cumulus cloud field indicates that particles stay in cloud as cloud droplets for about 23% of simulation time for "CF-Cloud" (versus 5% for "CF-All"). By considering both trajectory sets, we can simulate chemistry in the combined cloudy + clear sky between clouds ("CF-All") vs. only in-cloud trajectories ("CF-Cloud") and assess the contribution of in-cloud chemistry to MS and NSS production; our simulations suggest that in-cloud processes account for about 60% of MS and 56% of NSS production. These values are much lower than estimates for the stratocumulus trajectory sets. The contribution of in-cloud chemistry to MS and NSS production depends largely on the amount of cloud-free vs. cloudy area in the simulation field. In our simulations of stratocumulus clouds, the cloud covers the whole simulation area. But for the cumulus simulations, only about 22% of simulation area is covered by cumulus clouds, which could be derived from the fraction of trajectories that pass through the cloud and the percentage in-cloud

residence times for “CF-Cloud” and “CF-All”. Results from the “CF-Cloud” trajectories will be used to represent the in-cloud processing for the cumulus convection.

Because of their shorter in-cloud residence time, one simulation cycle for “CF-Cloud” represents ~ 30 minutes in-cloud processing. For consistency, MS and NSS obtained from 20 simulation cycles for “CF-Cloud” trajectories are compared to those from 8 simulation cycles of “ASTEX-1”, both representing ~1.5 days of atmospheric in-cloud processing. As presented in Figure 6, both MS (Figure 6a) and NSS (Figure 6b) production from stratocumulus clouds are higher than those from “CF-Cloud”, while the difference between two trajectory sets is apparently more significant for NSS than for MS. For the same reason discussed in section 4.2.1, the higher liquid water content of the cumulus cloud, together with the shorter in-cloud residence time of cumulus trajectories result in much more efficient production of MS than NSS from the “CF-Cloud” simulation. As a result, MS/NSS for “CF-Cloud” obtained after 1.5 days of in-cloud processing in the “CF-Cloud” (0.95) is higher than that from “ASTEX-1” (0.44). Different temperatures in the two cloud fields are also important in determining MS/NSS ratios. As discussed in section 4.1.3, lower temperatures result in higher MS/NSS ratios under cloudy conditions. Stratocumulus clouds are primarily within the boundary layer; cumulus clouds are present at higher altitudes, where both pressure and temperature are lower than in the boundary layer. Thus cumulus trajectories favor the production of MS and lead to higher MS/NSS in the free troposphere.

4.3 Comparison with Field Observations and Implications of the Present Work

Comparing our results with field observations helps assess the applicability of our simulation to the atmosphere. Field measurements of MS and NSS as well as MS/NSS in

marine atmospheric aerosols vary significantly with location and season, because temperature, solar radiation, radical concentrations, and dynamics of the atmosphere can strongly affect DMS emissions and oxidation processes.

It is worth noting that the MS/NSS ratio simulated from our model represents the value that will be observed when the oxidation of local oceanic DMS is the only source of MS and NSS (when the mechanism in Figure 1 is applied under the conditions considered). However, in field observations, both vertical and horizontal transport of sulfur compounds originating from other sources play important roles in the observed levels of the DMS oxidation products. In two recent missions to investigate sulfur chemistry in the Antarctic Troposphere (ISCAT), MS/NSS ratios of 0.06 and 0.05 were observed at the South Pole [*Arimoto, et al.*, 2001; *Davis, et al.*, 2004], close to the value of 0.07-0.08 observed in the tropical areas [*Davis, et al.*, 1999; *Saltzman, et al.*, 1983]. These observations are in conflict with our simulations at different temperatures. Our simulations suggest that the MS/NSS ratio increases with decreasing temperature, so MS/NSS in the South Pole is expected to be higher than that observed in the equatorial areas. However, in the atmosphere, the variation in temperature often induces variations in radical concentrations, physical properties of clouds, as well as the emission rate of DMS and sea-salt from the ocean, which are not considered in our assessment. Hence, our assessment of temperature dependence of MS/NSS represents purely the temperature effect on MS and NSS production rate from DMS oxidation. Meanwhile, extremely low DMS concentrations observed at the South Pole suggest that the observed sulfur compounds are primarily from long range transport of oceanic emissions. Thus, oxidation of DMS at different locations and altitudes is potentially responsible for the observed levels of MS and NSS, and it is quite likely that the chemistry mechanism of DMS oxidation varies with location and altitude.

For example, the oxidation of S(IV) by O_3 in alkaline sea-salt aerosols was found to proceed rapidly and explain the high levels of NSS-SO_4^{2-} observed in sea-salt aerosols [*Alexander, et al.*, 2005; *Chameides and Stelson*, 1992; *Sievering, et al.*, 2004]. However, this effect was not considered in our simulations. As a result, the simulated MS/NSS from our model tend to be higher than the field measurements under similar conditions.

In the studies from *Davis et al*. [1998] in the Antarctic, numerous abrupt enhancements were seen in the mixing ratios of gas-phase DMSO and DMSO2, which were speculated to be from the frequent episodes of rapid vertical transport between the very shallow boundary layer and the overlying "buffer layer". Due to the combination of long photochemical lifetime of DMS and the frequency of shallow convective events, a large fraction of oceanic DMS is transported into the "buffer layer" before being oxidized. In the "buffer layer", oxidized sulfur compounds accumulate due to lower humidity and aerosol concentration. Meanwhile, photo-oxidation becomes the dominant sink for DMSO, leading to higher production of SO_2 and H_2SO_4; thus nucleation of H_2SO_4 is possible to form fine particles within the "buffer layer". On the other hand, given the very low water vapor pressure in the "buffer layer", MSA is more likely to evaporate from the dry particles than H_2SO_4 when they are transported into the "buffer layer" from the boundary layer (*R. J. Weber,* private communication). As a result, when these particles are re-entrained into the boundary layer, the MS/NSS ratio in particles is evidently reduced while higher levels of DMSO, DMSO2 and MSA in the gas phase are observed.

Despite the differences and uncertainties discussed above, our simulated MS concentration of 0.7-0.8 nmol m^{-3} for the "ASTEX-1" and "ASTEX-2" clouds under PS conditions agree well with some field observations, e.g., studies in the equatorial Pacific by *Davis et al.* [1999] and in coastal Antarctica (summer) by *Jourdain* & *Legrand* [2001]. This

estimated MS level falls well within the often cited range except for the extremely low MS levels observed at coastal Antarctica [e.g., *Jourdain and Legrand*, 2001] and at the South Pole [e.g., *Arimoto, et al.*, 2001; *Davis, et al.*, 2004]. Conversely, our estimate of 2.0-3.5 nmol m^{-3} for NSS from these simulations is at the lower end of field measurements, such as those obtained in Antarctica and the South Pole, and is about a factor of 15 to 30 lower than anthropogenically influenced coastal areas [e.g., *Bardouki, et al.*, 2003; e.g., *Putaud, et al.*, 1999]. The only source of NSS in our simulation is DMS oxidation, while production of NSS from other sources cannot be ruled out in any field measurements. Even at the pristine South Pole, non-biogenic contributions to NSS (mainly from volcanoes and long range transport from the upper troposphere and stratosphere) could be as high as 35% [*Arimoto, et al.*, 2001]. Our simulated SO_2(g) achieves a steady-state concentration of ~ 6 pptv after ~ 10 simulation cycles, which is much lower than the typical value of ~ 40 pptv in the unpolluted marine atmosphere [*Berresheim, et al.*, 1993; *Davis, et al.*, 1999; *Jourdain and Legrand*, 2001; *Seinfeld and Pandis*, 1998]. As discussed in section 3.2, the simulated NSS increases by about 90% and 130% when initial SO_2 concentrations of 40 and 60 pptv are used, respectively. Other factors influencing NSS formation include long range transport, variable oxidant concentrations, variations in temperature, aerosol acidity, solar radiation and cloud coverage. These results further demonstrate that production of NSS from sources other than DMS oxidation may contribute to the difference between our simulations and field observations.

The steady-state MS/NSS is 0.35 and 0.21 from our simulations of the "ASTEX-1" and "ASTEX-2" stratocumulus clouds, and it decreases to ~ 0.12 for clear sky conditions (which could be approximately simulated from scenario GM). Therefore, we report a range between 0.1 and 0.4 as the MS/NSS ratio from our simulations. In a recent study by *Gondwe et al.*

[2004], over 50 observed MS/NSS ratios resulting from solely an oceanic DMS source of MS and NSS were listed. Given quite different conditions, including locations, temperatures, radical concentrations, solar radiation, DMS emissions, seasons, as well as the atmospheric dynamics during these numerous studies, a wide range in MS/NSS observations was found, and the average MS/NSS from all these studies is ~ 0.25. Our simulations suggest that atmospheric DMSO is likely always at "steady state" with DMS emissions, while SO_2 is not. As listed in Table 7, the simulated steady-state SO_2(g) concentration under cloud-free conditions is close to 50 pptv, which in itself might contribute to significant variability in the MS/NSS ratio observed in the atmosphere. However, the consistency between our estimate and the above average MS/NSS ratio further suggests that our model can represent the atmospheric DMS oxidation and MS and NSS production under typical global average marine atmospheric conditions.

5. Conclusions

In this work we incorporate DMS oxidation chemistry into the TEM to simulate MS and NSS production in the marine atmosphere. For the "ASTEX-1" and "ASTEX-2" stratocumulus clouds considered, the MS/NSS ratio is estimated to be 0.21-0.35. Under cloud free conditions, MS/NSS decreases to ~ 0.1, indicating that heterogeneous processes contribute more to MS than to NSS production. Our simulations suggest that aqueous phase transformations of sulfur compounds account for > 97% of MS and 83-95% of NSS production in particles. Oxidation of organo-sulfur species contributes ~ 30% and heterogeneous oxidation of S(IV) contributes over 60% to the total production of MS and NSS. For the first time, the oxidation of organic sulfur compounds by SO_4^-, Cl and Cl_2^- radicals are included in a model, and it is found that the MSI + Cl_2^- reaction is more important than MSI + OH as a pathway for MS production. The

temperature-dependent studies suggest that the MS/NSS ratio decreases with increasing temperature, which is potentially important for understanding observations of MS/NSS at different latitudes. The MS + OH reaction can reduce MS/NSS by 17% to 40% as temperature increases from 278 K to 318 K. Comparing simulations of trajectories in cumulus and stratocumulus clouds has found that MS/NSS produced from cumulus convection is higher than from stratocumulus clouds, which is potentially important in controlling the high concentration of MS and the MS/NSS ratios observed in the "buffer layer" by *Davis et al.* [1998].

Acknowledgements

A. Nenes acknowledges support from an NSF CAREER award, a Blanchard-Milliken Young Faculty Fellowship and GA Tech startup funds. The contributions of L. Zhu, J.M. Nicovich, and P.H. Wine were supported by NSF through grant ATM-03-50185. We would like to thank B. Stevens, G. Feingold and M-L Liu for providing trajectories.

References

Albrecht, B. A., C. S. Bretherton, D. Johnson, W. H. Scubert, and A. S. Frisch (1995), The Atlantic Atratocumulus Transition Experiment - ASTEX, *Bulletin of the American Meteorological Society*, *76*, 889-904.

Alexander, B., R. J. Park, D. J. Jacob, Q. B. Li, R. M. Yantosca, J. Savarino, C. C. W. Lee, and M. H. Thiemens (2005), Sulfate formation in sea-salt aerosols: Constraints from oxygen isotopes, *J. Geophys. Res.-Atmos.*, *110*, Art. No. D10307.

Amels, P., H. Elias, and K. J. Wannowius (1997), Kinetics and mechanism of the oxidation of dimethyl sulfide by hydroperoxides in aqueous medium - Study on the potential contribution of liquid-phase oxidation of dimethyl sulfide in the atmosphere, *J. Chem. Soc. Far. Trans.*, *93*, 2537-2544.

Arimoto, R., A. S. Nottingham, J. Webb, C. A. Schloesslin, and D. D. Davis (2001), Non-sea salt sulfate and other aerosol constituents at the South Pole during ISCAT, *Geophys. Res. Lett.*, *28*, 3645-3648.

Arsene, C., I. Barnes, and K. H. Becker (1999), FT-IR product study of the photo-oxidation of dimethyl sulfide: Temperature and O_2 partial pressure dependence, *Phys. Chem. Chem. Phys.*, *1*, 5463-5470.

Arsene, C., I. Barnes, K. H. Becker, W. F. Schneider, T. T. Wallington, N. Mihalopoulos, and I. V. Patroescu-Klotz (2002), Formation of methane sulfinic acid in the gas-phase OH-radical initiated oxidation of dimethyl sulfoxide, *Environ Sci Technol*, *36*, 5155-5163.

Atkinson, R., D. L. Baulch, R. A. Cox, J. N. Crowley, R. F. Hampson Jr., R. G. Hynes, M. E. Jenkin, J. A. Kerr, M. J. Rossi, and J. Troe (2004), IUPAC subcommittee on gas kinetic data evaluation for atmospheric chemistry, *Web Version July*.

Atkinson, R., D. L. Baulch, R. A. Cox, J. N. Crowley, R. F. Hampson, J. A. Kerr, M. J. Rossi, and J. Troe (2002), Summary of evaluated kinetic and photochemical data for atmospheric chemistry., *Web Version*.

Atkinson, R., D. L. Baulch, R. A. Cox, J. N. Crowley, R. F. J. Hampson, J. A. Kerr, M. J. Rossi, and J. Troe (2001), Summary of evaluated kinetic and photochemical data for atmospheric chemistry: IUPAC subcommittee on gas kinetic data evaluation for atmospheric chemistry web version December 2001, 1-56.

Atkinson, R., D. L. Baulch, R. A. Cox, R. F. Hampson, J. A. Kerr, M. J. Rossi, and J. Troe (1997), Evaluated kinetic and photochemical data for atmospheric chemistry: Supplement VI - IUPAC subcommittee on gas kinetic data evaluation for atmospheric chemistry, *J Phys Chem Ref Data*, *26*, 1329-1499.

Ayers, G. P., J. M. Cainey, R. W. Gillett, E. S. Saltzman, and M. Hooper (1997), Sulfur dioxide and dimethyl sulfide in marine air at Cape Grim, Tasmania, *Tellus B*, *49*, 292-299.

Bardouki, H., H. Berresheim, M. Vrekoussis, J. Sciare, G. Kouvarakis, K. Oikonomou, J. Schneider, and N. Mihalopoulos (2003), Gaseous (DMS, MSA, SO_2, H_2SO_4 and DMSO) and particulate (sulfate and methanesulfonate) sulfur species over the northeastern coast of Crete, *Atmos. Chem. Phys.*, *3*, 1871-1886.

Bardouki, H., M. B. da Rosa, N. Mihalopoulos, W. U. Palm, and C. Zetzsch (2002), Kinetics and mechanism of the oxidation of dimethylsulfoxide (DMSO) and methanesulfinate (MSI^-) by OH radicals in aqueous medium, *Atmos. Environ.*, *36*, 4627-4634.

Barone, S. B., A. A. Turnipseed, and A. R. Ravishankara (1995), Role of adducts in the atmospheric oxidation of dimethyl sulfide, *Faraday Discussions*, 39-54.

Bates, T. S., R. J. Charlson, and R. H. Gammon (1987), Evidence for the climatic role of marine biogenic sulfur, *Nature*, *329*, 319-321.

Benkovitz, C. M., C. M. Berkowitz, R. C. Easter, S. Nemesure, R. Wagener, and S. E. Schwartz (1994), Sulfate over the north-Atlantic and adjacent continental regions - Evaluation for October and November 1986 using a 3-dimensional model-driven by observation-derived meteorology, *J. Geophys. Res. - Atmos.*, *99*, 20725-20756.

Berresheim, H., F. L. Eisele, D. J. Tanner, L. M. Mcinnes, D. C. Ramseybell, and D. S. Covert (1993), Atmospheric sulfur chemistry and cloud condensation nuclei (CCN) concentrations over the Northeastern Pacific coast, *J. Geophys. Res. - Atmos.*, *98*, 12701-12711.

Betterton, E. A. (1992), Henry's law constants of soluble and moderately soluble organic gases: Effects on aqueous phase chemistry, *Adv. Environ. Sci. Tech.*, *24*, 1-50.

Bonifacic, M., H. Mockel, D. Bahnemann, and K. D. Asmus (1975), Formation of positive-ions and other primary species in oxidation of sulfides by hydroxyl radicals, *J. Chem. Soc. Perk. Trans. 2*, 675-685.

Botha, C. F., J. Hahn, J. J. Pienaar, and R. Vaneldik (1994), Kinetics and mechanism of the oxidation of sulfur(IV) by ozone in aqueous-solutions, *Atmos. Environ.*, *28*, 3207-3212.

Boucher, O., C. Moulin, S. Belviso, O. Aumont, L. Bopp, E. Cosme, R. von Kuhlmann, M. G. Lawrence, M. Pham, M. S. Reddy, J. Sciare, and C. Venkataraman (2003), DMS atmospheric concentrations and sulphate aerosol indirect radiative forcing: a sensitivity study to the DMS source representation and oxidation, *Atmos. Chem. Phys.*, *3*, 49-65.

Campolongo, F., A. Saltelli, N. R. Jensen, J. Wilson, and J. Hjorth (1999), The role of multiphase chemistry in the oxidation of dimethylsulphide (DMS). A latitude dependent analysis, *J. Atmos. Chem.*, *32*, 327-356.

Capaldo, K. P., and S. N. Pandis (1997), Dimethylsulfide chemistry in the remote marine atmosphere: Evaluation and sensitivity analysis of available mechanisms, *J. Geophys. Res. - Atmos.*, *102*, 23251-23267.

Chameides, W. L. (1984), The Photochemistry of a remote marine stratiform cloud, *J. Geophys. Res. - Atmos.*, *89*, 4739-4755.

Chameides, W. L., and A. W. Stelson (1992), Aqueous-phase chemical processes in deliquescent seasalt aerosols, *Ber. Bunsen - Ges. - Phys. Chem. Chem. Phys.*, *96*, 461-470.

Charlson, R. J., J. E. Lovelock, M. O. Andreae, and S. G. Warren (1987), Oceanic phytoplankton, atmospheric sulfur, cloud albedo and climate, *Nature*, *326*, 655-661.

Chen, G., D. D. Davis, P. Kasibhatla, A. R. Bandy, D. C. Thornton, B. J. Huebert, A. D. Clarke, and B. W. Blomquist (2000), A study of DMS oxidation in the tropics: Comparison of christmas island field observations of DMS, SO_2, and DMSO with model simulations, *J. Atmos. Chem.*, *37*, 137-160.

Chin, M., R. B. Rood, S. J. Lin, J. F. Muller, and A. M. Thompson (2000a), Atmospheric sulfur cycle simulated in the global model GOCART: Model description and global properties, *J. Geophys. Res. - Atmos.*, *105*, 24671-24687.

Chin, M., D. L. Savoie, B. J. Huebert, A. R. Bandy, D. C. Thornton, T. S. Bates, P. K. Quinn, E. S. Saltzman, and W. J. De Bruyn (2000b), Atmospheric sulfur cycle simulated in the global model GOCART: Comparison with field observations and regional budgets, *J. Geophys. Res. - Atmos.*, *105*, 24689-24712.

Clarke, J. H. R., and L. A. Woodward (1966), Raman spectrophotometric determination of degrees of dissociation of methanesulphonic acid in aqueous solution at 25 degrees C, *T Faraday Soc*, *62*, 2226-2233.

Conant, W. C., T. M. VanReken, T. A. Rissman, V. Varutbangkul, H. H. Jonsson, A. Nenes, J. L. Jimenez, A. E. Delia, R. Bahreini, G. C. Roberts, R. C. Flagan, and J. H. Seinfeld (2004), Aerosol-cloud drop concentration closure in warm cumulus, *J. Geophys. Res. - Atmos.*, *109*, D13204, doi: 13210.11029/ 12003JD004324.

Cosme, E., C. Genthon, P. Martinerie, O. Boucher, and M. Pham (2002), The sulfur cycle at high-southern latitudes in the LMD-ZT general circulation model, *J. Geophys. Res. - Atmos.*, *107*, 4690-4708.

Davis, D., G. Chen, A. Bandy, D. Thornton, F. Eisele, L. Mauldin, D. Tanner, D. Lenschow, H. Fuelberg, B. Huebert, J. Heath, A. Clarke, and D. Blake (1999), Dimethyl sulfide oxidation in the equatorial Pacific: Comparison of model simulations with field observations for DMS, SO_2, H_2SO_4(g), MSA(g), MS, and NSS, *J. Geophys. Res.-Atmos.*, *104*, 5765-5784.

Davis, D., G. Chen, P. Kasibhatla, A. Jefferson, D. Tanner, F. Eisele, D. Lenschow, W. Neff, and H. Berresheim (1998), DMS oxidation in the Antarctic marine boundary layer: Comparison of model simulations and field observations of DMS, DMSO, DMSO2, H_2SO_4(g), MSA(g), and MSA(p), *J. Geophys. Res.- Atmos.*, *103*, 1657-1678.

Davis, D. D., F. Eisele, G. Chen, J. Crawford, G. Huey, D. Tanner, D. Slusher, L. Mauldin, S. Oncley, D. Lenschow, S. Semmer, R. Shetter, B. Lefer, R. Arimoto, A. Hogan, P. Grube, M. Lazzara, A. Bandy, D. Thornton, H. Berresheim, H. Bingemer, M. Hutterli, J. McConnell, R. Bales, J. Dibb, M. Buhr, J. Park, P. McMurry, A. Swanson, S. Meinardi, and D. Blake (2004), An overview of ISCAT 2000, *Atmos. Environ.*, *38*, 5363-5373.

De Bruyn, W. J., T. S. Bates, J. M. Cainey, and E. S. Saltzman (1998), Shipboard measurements of dimethyl sulfide and SO_2 southwest of Tasmania during the First Aerosol Characterization Experiment (ACE 1), *J. Geophys. Res. - Atmos.*, *103*, 16703-16711.

De Bruyn, W. J., M. Harvey, J. M. Cainey, and E. S. Saltzman (2002), DMS and SO_2 at Baring Head, New Zealand: Implications for the yield of SO_2 from DMS, *J. Atmos. Chem.*, *41*, 189-209.

De Bruyn, W. J., J. A. Shorter, P. Davidovits, D. R. Worsnop, M. S. Zahniser, and C. E. Kolb (1994), Uptake of gas-phase sulfur species methanesulfonic-acid, dimethylsulfoxide, and dimethyl sulfone by aqueous surfaces, *J. Geophys. Res. - Atmos.*, *99*, 16927-16932.

Erickson, R. E., L. M. Yates, R. L. Clark, and D. Mcewen (1977), Reaction of sulfur-dioxide with ozone in water and its possible atmospheric significance, *Atmos. Environ.*, *11*, 813-817.

Gershenzon, M., P. Davidovits, J. T. Jayne, C. E. Kolb, and D. R. Worsnop (2001), Simultaneous uptake of DMS and ozone on water, *J. Phys. Chem. A*, *105*, 7031-7036.

Gmehling, J., P. Rasmussen, and A. Fredenslund (1982), Vapor-liquid-equilibria by unifac group contribution - Revision and extension.2., *Ind Eng Chem Proc Dd*, *21*, 118-127.

Gondwe, M., M. Krol, W. Gieskes, W. Klaassen, and H. de Baar (2003), The contribution of ocean-leaving DMS to the global atmospheric burdens of DMS, MSA, SO_2, and NSS $SO_4^=$, *Global Biogeochemical Cycles*, *17*, 1056, doi: 1010.1029/ 2002GB001937.

Gondwe, M., M. Krol, W. Klaassen, W. Gieskes, and H. de Baar (2004), Comparison of modeled versus measured MSA: nss $SO_4^=$ ratios: A global analysis, *Global Biogeochemical Cycles*, *18*, GB2006, doi: 2010.1029/2003GB002144.

Herrmann, H., B. Ervens, H. W. Jacobi, R. Wolke, P. Nowacki, and R. Zellner (2000), CAPRAM2.3: A chemical aqueous phase radical mechanism for tropospheric chemistry, *J. Atmos. Chem.*, *36*, 231-284.

Herrmann, H., H. W. Jacobi, G. Raabe, A. Reese, and R. Zellner (1996), Laser-spectroscopic laboratory studies of atmospheric aqueous phase free radical chemistry, *Fresen J Anal Chem*, *355*, 343-344.

Hertel, O., J. Christensen, and O. Hov (1994), Modeling of the end-products of the chemical decomposition of DMS in the Marine Boundary Layer, *Atmos. Environ.*, *28*, 2431-2449.

Hoffmann, M. R. (1986), On the kinetics and mechanism of oxidation of aquated sulfur-dioxide by ozone, *Atmos. Environ.*, *20*, 1145-1154.

Hynes, A. J., R. E. Stickel, A. J. Pounds, Z. Zhao, T. Mckay, J. D. Bradshaw, and P. H. Wine (1993), Mechanistic studies of the OH-initiated oxidation of dimethylsulfide, in *Dimethylsulfide: Oceans, Atmosphere and Climate*, edited by G. Restelli and G. Angeletti, pp. 211-221, Kluwer Academic Publishers.

Hynes, A. J., P. H. Wine, and D. H. Semmes (1986), Kinetics and mechanism of OH reactions with organic sulfides, *J. Phys. Chem.*, *90*, 4148-4156.

Ingham, T., D. Bauer, R. Sander, P. J. Crutzen, and J. N. Crowley (1999), Kinetics and products of the reactions BrO+DMS and Br+DMS at 298 K, *J. Phys. Chem. A*, *103*, 7199-7209.

Jaegle, L., D. J. Jacob, W. H. Brune, I. Faloona, D. Tan, B. G. Heikes, Y. Kondo, G. W. Sachse, B. Anderson, G. L. Gregory, H. B. Singh, R. Pueschel, G. Ferry, D. R. Blake, and R. E. Shetter (2000), Photochemistry of HOx in the upper troposphere at northern midlatitudes, *J. Geophys. Res. - Atmos.*, *105*, 3877-3892.

Jourdain, B., and M. Legrand (2001), Seasonal variations of atmospheric dimethylsulfide, dimethylsulfoxide, sulfur dioxide, methanesulfonate, and non-sea-salt sulfate aerosols at Dumont d'Urville (coastal Antarctica) (December 1998 to July 1999), *J. Geophys. Res. - Atmos.*, *106*, 14391-14408.

Katoshevski, D., A. Nenes, and J. H. Seinfeld (1999), A study of processes that govern the maintenance of aerosols in the marine boundary layer, *J. Aerosol Sci.*, *30*, 503-532.

Koga, S., and H. Tanaka (1993), Numerical study of the oxidation process of Dimethylsulfide in the marine atmosphere, *J. Atmos. Chem.*, *17*, 201-228.

Kreidenweis, S. M., J. E. Penner, F. Yin, and J. H. Seinfeld (1991), The effects of Dimethylsulfide upon marine aerosol concentrations, *Atmos. Environ.*, *25*, 2501-2511.

Kreidenweis, S. M., C. J. Walcek, G. Feingold, W. M. Gong, M. Z. Jacobson, C. H. Kim, X. H. Liu, J. E. Penner, A. Nenes, and J. H. Seinfeld (2003), Modification of aerosol mass and size distribution due to aqueous-phase SO_2 oxidation in clouds: Comparisons of several models, *J. Geophys. Res. - Atmos.*, *108*, 4213, doi:4210.1029/2002JD002697.

Kukui, A., D. Borissenko, G. Laverdet, and G. Le Bras (2003), Gas-phase reactions of OH radicals with dimethyl sulfoxide and methane sulfinic acid using turbulent flow reactor and chemical ionization mass spectrometry, *J. Phys. Chem. A*, *107*, 5732-5742.

Lagrange, J., C. Pallares, and P. Lagrange (1994), Electrolyte effects on aqueous atmospheric oxidation of sulfur-dioxide by ozone, *J. Geophys. Res. - Atmos.*, *99*, 14595-14600.

Lee, Y. N., and X. L. Zhou (1994), Aqueous reaction-Kinetics of ozone and Dimethylsulfide and its atmospheric implications, *J. Geophys. Res. - Atmos.*, *99*, 3597-3605.

Legrand, M., J. Sciare, B. Jourdain, and C. Genthon (2001), Subdaily variations of atmospheric dimethylsulfide, dimethylsulfoxide, methanesulfonate, and non-sea-salt sulfate aerosols in

the atmospheric boundary layer at Dumont d'Urville (coastal Antarctica) during summer, *J. Geophys. Res. - Atmos.*, *106*, 14409-14422.

Lelieveld, J., and P. J. Crutzen (1991), The role of clouds in tropospheric photochemistry, *J. Atmos. Chem.*, *12*, 229-267.

Lind, J., and T. E. Eriksen (1975), Pulse-radiolysis of Methane Sulfonic Acid, *Radiochem. Radioanal. Lett.*, *21*, 177-181.

Mari, C., K. Suhre, R. Rosset, T. S. Bates, B. J. Huebert, A. R. Bandy, D. C. Thornton, and S. Businger (1999), One-dimensional modeling of sulfur species during the First Aerosol Characterization Experiment (ACE 1) Lagrangian B, *J. Geophys. Res. - Atmos.*, *104*, 21733-21749.

Martinez, E., J. Albaladejo, E. Jimenez, A. Notario, and A. Aranda (1999), Kinetics of the reaction of CH_3S with NO_2 as a function of temperature, *Chemical Physics Letters*, *308*, 37-44.

Martinez, E., J. Albaladejo, A. Notario, and E. Jimenez (2000), A study of the atmospheric reaction of CH_3S with O_3 as a function of temperature, *Atmos. Environ.*, *34*, 5295-5302.

Medina, J. A., and A. Nenes (2004), Effects of film forming compounds on the growth of Giant CCN: Implications for cloud microphysics and the aerosol indirect effect, *J. Geophys. Res.*, *109*, D20207, doi:20210.21029/22004JD004666.

Milne, P. L., R. G. Zika, and E. S. Saltzmann (1989), Rate of reaction of methanesulfonic acid, dimethyl sulfoxide, and dimethyl sulfone with hydroxyl radical in aqueous solution., in *Biogenic Sulfur in the Environment*, edited by E. S. Saltzmanm and W. J. Cooper, pp. 518-528.

Nahir, T. M., and G. A. Dawson (1987), Oxidation of sulfur-dioxide by ozone in highly dispersed water droplets, *J. Atmos. Chem.*, *5*, 373-383.

Nakano, Y., M. Goto, S. Hashimoto, M. Kawasaki, and T. J. Wallington (2001), Cavity ring-down spectroscopic study of the reactions of Br atoms and BrO radicals with dimethyl sulfide, *J. Phys. Chem. A*, *105*, 11045-11050.

Noxon, J. F. (1983), NO_3 and NO_2 in the Mid-Pacific Troposphere, *J. Geophys. Res.*, *88*, 1017-1021.

Olson, T. M., and R. W. Fessenden (1992), Pulse-radiolysis study of the reaction of OH-bullet radicals with Methanesulfonate and Hydroxymethanesulfonate, *J. Phys. Chem.*, *96*, 3317-3320.

Pham, M., J. F. Muller, G. P. Brasseur, C. Granier, and G. Megie (1995), A three-dimensional study of the tropospheric sulfur cycle, *J. Geophys. Res. - Atmos.*, *100*, 26061-26092.

Poschl, U., M. Canagaratna, J. T. Jayne, L. T. Molina, D. R. Worsnop, C. E. Kolb, and M. J. Molina (1998), Mass accommodation coefficient of H_2SO_4 vapor on aqueous sulfuric acid surfaces and gaseous diffusion coefficient of H_2SO_4 in N_2/H_2O, *J. Phys. Chem. A*, *102*, 10082-10089.

Prinn, R. G., R. F. Weiss, B. R. Miller, J. Huang, F. N. Alyea, D. M. Cunnold, P. J. Fraser, D. E. Hartley, and P. G. Simmonds (1995), Atmospheric trends and lifetime of CH_3CCl_3 and global OH concentrations, *Science*, *269*, 187-192.

Pryor, W. A., D. H. Giamalva, and D. F. Church (1984), Kinetics of ozonation.2. Amino-acids and model compounds in water and comparisons to rates in nonpolar-solvents, *J Am Chem Soc*, *106*, 7094-7100.

Pszenny, A. A. P., W. C. Keene, D. J. Jacob, S. Fan, J. R. Maben, M. P. Zetwo, M. Springeryoung, and J. N. Galloway (1993), Evidence of inorganic chlorine gases other than hydrogen-chloride in marine surface air, *Geophys. Res. Lett.*, *20*, 699-702.

Putaud, J. P., B. M. Davison, S. F. Watts, N. Mihalopoulos, B. C. Nguyen, and C. N. Hewitt (1999), Dimethylsulfide and its oxidation products at two sites in Brittany (France), *Atmos. Environ.*, *33*, 647-659.

Reuvers, A. P., Greensto.Cl, J. Borsa, and J. D. Chapman (1973), Studies on mechanism of chemical radioprotection by Dimethyl Sulfoxide, *Int. J. Radiat. Biol.*, *24*, 533-536.

Saltzman, E. S., D. L. Savoie, R. G. Zika, and J. M. Prospero (1983), Methane Sulfonic-Acid in the marine atmosphere, *J. Geophys. Res.*, *88*, 897-902.

Sander, R., and P. J. Crutzen (1996), Model study indicating halogen activation and ozone destruction in polluted air masses transported to the sea, *J. Geophys. Res. - Atmos.*, *101*, 9121-9138.

Scaduto, R. C. (1995), Oxidation of DMSO and Methanesulfinic acid by the hydroxyl radical, *Free Radical Bio Med*, *18*, 271-277.

Sciare, J., M. Kanakidou, and N. Mihalopoulos (2000), Diurnal and seasonal variation of atmospheric dimethylsulfoxide at Amsterdam Island in the southern Indian Ocean, *J. Geophys. Res. - Atmos.*, *105*, 17257-17265.

Sehested, K., and J. Holcman (1996), A pulse radiolysis study of the OH radical induced autoxidation of methanesulfinic acid, *Radiat. Phys. Chem.*, *47*, 357-360.

Seinfeld, J. H. (1986), *Air Pollution*, Wiley and Sons, New York.

Seinfeld, J. H., and S. N. Pandis (1998), *Atmospheric Chemistry and Physics: From air pollution to climate change*, John Wiley & Sons, New York.

Shon, Z. H., D. Davis, G. Chen, G. Grodzinsky, A. Bandy, D. Thornton, S. Sandholm, J. Bradshaw, R. Stickel, W. Chameides, G. Kok, L. Russell, L. Mauldin, D. Tanner, and F. Eisele (2001), Evaluation of the DMS flux and its conversion to SO_2 over the southern ocean, *Atmos. Environ.*, *35*, 159-172.

Sievering, H., J. Cainey, M. Harvey, J. McGregor, S. Nichol, and P. Quinn (2004), Aerosol non-sea-salt sulfate in the remote marine boundary layer under clear-sky and normal cloudiness conditions: Ocean-derived biogenic alkalinity enhances sea-salt sulfate production by ozone oxidation, *J. Geophys. Res-Atmos.*, *109*, Art. No. D19317.

Stevens, B., G. Feingold, W. R. Cotton, and R. L. Walko (1996), Elements of the microphysical structure of numerically simulated nonprecipitating stratocumulus, *J Atmos Sci*, *53*, 980-1006.

Tan, D., I. Faloona, J. B. Simpas, W. Brune, J. Olson, J. Crawford, M. Avery, G. Sachse, S. Vay, S. Sandholm, H. W. Guan, T. Vaughn, J. Mastromarino, B. Heikes, J. Snow, J. Podolske, and H. Singh (2001), OH and HO_2 in the tropical Pacific: Results from PEM-Tropics B, *J. Geophys. Res. - Atmos.*, *106*, 32667-32681.

Turnipseed, A. A., S. B. Barone, and A. R. Ravishankara (1993), Reactions of CH_3S and CH_3SOO with O_3, NO_2, and NO, *J. Phys. Chem.*, *97*, 5926-5934.

Turnipseed, A. A., S. B. Barone, and A. R. Ravishankara (1996), Reaction of OH with dimethyl sulfide 2. Products and mechanisms, *J. Phys. Chem.*, *100*, 14703-14713.

Tyndall, G. S., R. A. Cox, C. Granier, R. Lesclaux, G. K. Moortgat, M. J. Pilling, A. R. Ravishankara, and T. J. Wallington (2001), Atmospheric chemistry of small organic peroxy radicals, *J. Geophys. Res. - Atmos.*, *106*, 12157-12182.

Tyndall, G. S., and A. R. Ravishankara (1989a), Atmospheric reactions of CH_3S radicals, *ACS Symposium Series*, *393*, 450-458.

Tyndall, G. S., and A. R. Ravishankara (1989b), Kinetics of the reaction of CH_3S with O_3 at 298-K, *J. Phys. Chem.*, *93*, 4707-4710.

Urbanski, S. P., R. E. Stickel, and P. H. Wine (1998), Mechanistic and kinetic study of the gas-phase reaction of hydroxyl radical with dimethyl sulfoxide, *J. Phys. Chem. A*, *102*, 10522-10529.

Urbanski, S. P., R. E. Stickel, Z. Z. Zhao, and P. H. Wine (1997), Mechanistic and kinetic study of formaldehyde production in the atmospheric oxidation of dimethyl sulfide, *J. Chem. Soc. Far. Trans.*, *93*, 2813-2819.

Urbanski, S. P., and P. H. Wine (1999), Chemistry of gas phase organic sulfur-centered radicals, in *S-Centered Radicals*, edited by Z. B. Alfassi, pp. 97-140, John Wiley and Sons.

Veltwisch, D., E. Janata, and K. D. Asmus (1980), Primary processes in the reaction of OH-radicals with sulfoxides, *J. Chem. Soc. Perk. Trans. 2*, 146-153.

Vogt, R., P. J. Crutzen, and R. Sander (1996), A mechanism for halogen release from sea-salt aerosol in the remote marine boundary layer, *Nature*, *383*, 327-330.

von Glasow, R., and P. J. Crutzen (2004), Model study of multiphase DMS oxidation with a focus on halogens, *Atmos. Chem. Phys.*, *4*, 589-608.

Weast, R. C. (1980), *CRC Handbook of Chemistry and Physics, 61 st Edition*, CRC Press, Inc., Boca Raton, FL.

Williams, M. B., P. Campuzano-Jost, D. Bauer, and A. J. Hynes (2001), Kinetic and mechanistic studies of the OH-initiated oxidation of dimethylsulfide at low temperature - A

reevaluation of the rate coefficient and branching ratio, *Chemical Physics Letters*, *344*, 61-67.

Wine, P. H., R. J. Thompson, A. R. Ravishankara, D. H. Semmes, C. A. Gump, A. Torabi, and J. M. Nicovich (1984), Kinetics of the reaction $OH+SO_2+M$ ---> $HOSO_2+M$. Temperature and pressure-dependence in the falloff region, *J. Phys. Chem.*, *88*, 2095-2104.

Wingenter, O. W., M. K. Kubo, N. J. Blake, T. W. Smith, D. R. Blake, and F. S. Rowland (1996), Hydrocarbon and halocarbon measurements as photochemical and dynamical indicators of atmospheric hydroxyl, atomic chlorine, and vertical mixing obtained during Lagrangian flights, *J. Geophys. Res. - Atmos.*, *101*, 4331-4340.

Wudl, F., D. A. Lightner, and D. J. Cram (1967), Methanesulfinic Acid and Its Properties, *J. American Chem. Soc.*, *89*, 4099-4101.

Yin, F. D., D. Grosjean, R. C. Flagan, and J. H. Seinfeld (1990a), Photooxidation of Dimethyl Sulfide and Dimethyl Disulfide.2. Mechanism evaluation, *J. Atmos. Chem.*, *11*, 365-399.

Yin, F. D., D. Grosjean, and J. H. Seinfeld (1990b), Photooxidation of Dimethyl Sulfide and Dimethyl Disulfide.1. Mechanism development, *J. Atmos. Chem.*, *11*, 309-364.

Yu, X. Y., Z. C. Bao, and J. R. Barker (2004), Free radical reactions involving Cl, Cl_2^-, and SO_4^- in the 248 nm photolysis of aqueous solutions containing $S_2O_8^{2-}$ and Cl^-, *J. Phys. Chem. A*, *108*, 295-308.

Zhu, L., J. M. Nicovich, and P. H. Wine (2003a), Temperature-dependent kinetics studies of aqueous phase reactions of hydroxyl radicals with dimethylsulfoxide, dimethylsulfone, and methanesulfonate, *Aquatic Sci.*, *65*, 425-435.

Zhu, L., J. M. Nicovich, and P. H. Wine (2003b), Temperature-dependent kinetics studies of aqueous phase reactions of SO_4^- radicals with dimethylsulfoxide, dimethylsulfone, and methanesulfonate, *J. Photochem. Photobio. A - Chem.*, *157*, 311-319.

Zhu, L., J. M. Nicovich, and P. H. Wine (2005), Kinetics studies of aqueous phase reactions of Cl atoms and Cl_2^- radicals with organic sulfur compounds of atmospheric interest, *J.Phys. Chem. A*, *109*, 3903-3911.

Table 1 Gas phase kinetic mechanism

#	Reaction	k (T) (cm^3 $molecule^{-1}$ s^{-1})	Source
G1	$CH_3SCH_3 + OH \xrightarrow{O_2} CH_3SCH_2O_2 + H_2O$	$1.13\times10^{-11}\exp(-253/T)$	*Atkinson et al.* [2001]
G2	$CH_3SCH_3 + OH \xrightarrow{O_2} 0.5CH_3S(O)CH_3 + 0.2CH_3(O)S(O)CH_3 + 0.3\ CH_3(O)SOH$	$\frac{1.0\times10^{-39}\exp(5820/T)[O_2]}{(1+5.0\times10^{-30}\exp(6280/T)[O_2])}$	*Hynes et al.* [1986], *Atkinson et al.* [1997], *Williams et al*. [2001], *Atkinson et al*. [2004]
G3	$CH_3SCH_3 + NO_3 \xrightarrow{O_2} CH_3SCH_2O_2 + HNO_3$	$1.9\times10^{-13}\exp(520/T)$	*Atkinson et al*. [2001]
G4	$CH_3SCH_3 + Cl \xrightarrow{O_2} CH_3SCH_2O_2 + HCl$	3.3×10^{-10}	*Atkinson et al*. [2001]
G5	$CH_3SCH_3 + BrO \rightarrow CH_3S(O)CH_3 + Br$	$1.4\times10^{-14}\exp(940/T)$	*Atkinson et al*. [1997], *Ingham et al*. [1999], *Nakano et al*. [2001]
G6	$CH_3SCH_2O_2 + NO \rightarrow CH_3S + CH_2O + NO_2$	$4.9\times10^{-12}\exp(260/T)$	*Urbanski et al.* [1997], *Atkinson et al*. [2001]
G7	$2CH_3SCH_2O_2 \rightarrow 2CH_3S + 2CH_2O + O_2$	1.0×10^{-11}	*Urbanski et al*. [1997], *Atkinson et al*. [2001]
G8	$CH_3SCH_2O_2 + HO_2 \rightarrow CH_3S$	$3.8\times10^{-13}\exp(780/T)$	[1]*Tyndall et al*.[2001]
G9	$CH_3S \xrightarrow{NO_2, O_3, HO_2, O_2, H_2O} 0.9\ SO_2 + 0.1\ H_2SO_4$	5.0	*Barone et al.* [1995], *Atkinson et al*. [2002]
G10	$CH_3S(O)CH_3 + OH \xrightarrow{O_2} 0.9\ CH_3(O)SOH + 0.1CH_3(O)S(O)CH_3$	9.0×10^{-11}	*Urbanski et al*. [1998], *Kukui et al*. [2003]
G11	$CH_3(O)SOH + OH \xrightarrow{O_2} 0.9SO_2 + 0.1\ CH_3(O)S(O)OH$	9.0×10^{-11}	*Kukui et al*. [2003]
G12	$SO_2 + OH + O_2 + H_2O \rightarrow H_2SO_4 + HO_2$	[2] $k_{12} = F\times k_0\times k_\infty/(k_0 + k_\infty)$	*Wine et al*. [1984]

[1] by analogy to $CH_3O_2 + HO_2$ [2] $\log F = \log(0.525)/(1 + [\log(k_0/k_\infty)]^2)$, where $k_0 = 4.5\times10^{-31}\ (T/300)^{-3.9}\times[Air]$, $k_\infty = 1.26\times10^{-12}\ (T/300)^{-0.7}$.

Table 2 Aqueous phase kinetic mechanism

#	Reaction	k (T) (M^{-1} s^{-1})	Source
A1	$CH_3SCH_3 + O_3 \rightarrow CH_3S(O)CH_3 + O_2$	5.3×10^{12} exp(-2600/T)	*Gershenzon et al*. [2001]
A2	$CH_3SCH_3 + OH \rightarrow CH_3S(O)CH_3 + HO_2$	1.9×10^{10}	*Bonifacic et al*. [1975]
A3	$CH_3S(O)CH_3 + O_3 \rightarrow CH_3(O)S(O)CH_3 + O_2$	5.7	*Lee and Zhou* [1994]
A4	$CH_3S(O)CH_3 + OH \rightarrow CH_3(O)SOH + CH_3$	4.7×10^{11} exp(-1270/T)	*Zhu et al*. [2003a]
A5	$CH_3S(O)CH_3 + SO_4^- \xrightarrow{H_2O} CH_3(O)SO^-$	3.7×10^{11} exp(-1440/T)	*Zhu et al*. [2003b]
A6	$CH_3S(O)CH_3 + Cl \xrightarrow{H_2O} CH_3(O)SO^-$	6.3×10^{9}	*Zhu et al [2005]*
A7	$CH_3S(O)CH_3 + Cl_2^- \xrightarrow{H_2O} CH_3(O)SO^-$	1.6×10^{7}	*Zhu et al [2005]*
A8	$CH_3(O)S(O)CH_3 + OH \rightarrow 0.3\ CH_3SO_3H + 0.7\ SO_4^{2-}$	5.1×10^{9} exp(-1690/T)	*Zhu et al*. [2003a]
A9	$CH_3(O)SO^- + OH \xrightarrow{O_2} CH_3(O)S(O)O^-$	7.7×10^{9}	*Zhu et al*. [2003a]
A10	$CH_3(O)SO^- + SO_4^- \xrightarrow{O_2} CH_3(O)S(O)O^-$	1.0×10^{9}	*Zhu et al*. [2003b]
A11	$CH_3(O)SO^- + Cl_2^- \xrightarrow{O_2} CH_3(O)S(O)O^-$	8.0×10^{8}	*Zhu et al [2005]*
A12	$CH_3(O)S(O)O^- + OH \rightarrow SO_4^{2-}$	8.8×10^{10} exp(-2630/T)	*Zhu et al [2005]*
A13	$SO_2 + O_3 \xrightarrow{H_2O} SO_4^{2-}$	2.4×10^{4}	*Kreidenweis et al*. [2003]
A14	$HSO_3^- + O_3 \xrightarrow{H_2O} SO_4^{2-}$	3.5×10^{5} exp[-5530(1/T-1/298)]	*Hoffmann* [1986], *Kreidenweis et al*. [2003]
A15	$SO_3^{2-} + O_3 \xrightarrow{H_2O} SO_4^{2-}$	1.5×10^{9} exp[-5280(1/T-1/298)]	*Hoffmann* [1986], *Kreidenweis et al*. [2003]
A16	$HSO_3^- + H_2O_2 \rightarrow SO_4^{2-}$	$\frac{7.45\times10^{7}\exp[-4430(1/T-1/298)]}{1+13[H^+]}$	*Hoffmann* [1986], *Kreidenweis et al.* [2003]

Table 3 Acid-base equilibria for aqueous phase species

#	Equilinrium Reaction	Equilibrium Constant (M)	Source
E1	$H_2SO_4 \leftrightarrow HSO_4^- + H^+$	1000	*Seinfeld* and *Pandis* [1998]
E2	$HSO_4^- \leftrightarrow SO_4^{2-} + H^+$	$1.02\times10^{-2}\exp[2720(1/T-1/298)]$	*Weast* [1980]
E3	$SO_2 + H_2O \leftrightarrow HSO_3^- + H^+$	$1.3\times10^{-2}\exp[1960(1/T-1/298)]$	*Chameides* [1984]
E4	$HSO_3^- \leftrightarrow SO_3^{2-} + H^+$	$6.6\times10^{-8}\exp[1500(1/T-1/298)]$	*Chameides* [1984]
E5	$H_2O_2 \leftrightarrow HO_2^- + H^+$	$2.2\times10^{-12}\exp[-3730(1/T-1/298)]$	*Kreidenweis et al*. [2003]
E6	$CO_2 + H_2O \leftrightarrow HCO_3^- + H^+$	$4.3\times10^{-7}\exp[-1000(1/T-1/298)]$	*Chameides* [1984]
E7	$HCO_3^- \leftrightarrow CO_3^{2-} + H^+$	$4.68\times10^{-11}\exp[-1760(1/T-1/298)]$	*Chameides* [1984]
E8	$NH_3 + H_2O \leftrightarrow NH_4^+ + OH^-$	$1.7\times10^{-5}\exp[-4500(1/T-1/298)]$	*Chameides* [1984]
E9	$CH_3SO_2H \leftrightarrow CH_3SO_2^- + H^+$	5.0×10^{-3}	*Wudl et al*. [1967]
E10	$CH_3S(O)_3H \leftrightarrow CH_3SO_3^- + H^+$	73	*Clarke and Woodward* [1966]

Table 4 Henry's Law's constant (H) and Mass Accommodation Coefficient (α) for semi-volatile species

Species	H ($M\ atm^{-1}$)	Source	Accommodation Coefficient	Source
SO_2	$1.23\ \exp[3140(1/T-1/298)]$	*Seinfeld* [1986]	0.035	*Kreidenweis et al*. [2003]
O_3	$1.1\times10^{-2}\ \exp[2540(1/T-1/298)]$	*Seinfeld* [1986]	5.3×10^{-4}	*Kreidenweis et al*. [2003]
H_2O_2	$7.45\times10^{4}\ \exp[7300(1/T-1/298)]$	*Seinfeld* [1986]	0.018	*Kreidenweis et al*. [2003]
HNO_3	$2.1\times10^{5}\ \exp[8700(1/T-1/298)]$	*Lelieveld* and *Crutzen* [1991]	0.05	*Kreidenweis et al*. [2003]
CO_2	$3.4\times10^{-2}\ \exp[2440(1/T-1/298)]$	*Seinfeld* [1986]	0.05	*Kreidenweis et al*. [2003]
NH_3	$62\ \exp[4110(1/T-1/298)]$	*Seinfeld* [1986]	0.05	*Kreidenweis et al*. [2003]
CH_3SCH_3	$0.56\ \exp[4480(1/T-1/298)]$	*Campolongo et al.* [1999]	0.001	Estimated
$CH_3S(O)CH_3$	$1.0\times10^{7}\ \exp[2580(1/T-1/298)]$	*Campolongo et al.* [1999]	0.1	*De Bruyn et al*. [1994]
$CH_3S(O)_2CH_3$	$1.0\times10^{7}\ \exp[5390(1/T-1/298)]$	*Campolongo et al.* [1999]	0.1	*De Bruyn et al*. [1994]
CH_3SO_2H	$1.0\times10^{9}\ \exp[1760(1/T-1/298)]$	*Campolongo et al*. [1999]	0.1	Assumed same as MSA
CH_3SO_3H	$1.0\times10^{9}\ \exp[1760(1/T-1/298)]$	*Campolongo et al.* [1999]	0.1	*De Bruyn et al*. [1994]
H_2SO_4	∞	*Campolongo et al*. [1999]	0.75	*Poschl et al*. [1998]

Table 5 Concentrations of steady-state radicals used in the simulation

Radicals	Concentration[#]	Source
OH(g)	1×10^{6}	*Prinn et al*. [1995]
NO_3(g)	1×10^{6}	*Noxon* [1983]
Cl(g)	1×10^{4}	*Pszenny et al.* [1993], *Wingenter et al*.[1996]
BrO(g)	1×10^{7}	*Sander* and *Crutzen* [1996], Vogt et al.[1996], *von Glasow* & *Crutzen* [2004]
NO (g)	1×10^{8}	*Seinfeld* and *Pandis*[1998]
HO_2 (g)	1×10^{8}	*Jaegle et al*. [2000], *Tan et al*. [2001]
OH (aq)	6×10^{-13}	*Herrmann et al*. [2000]
SO_4^-(aq)	1×10^{-12}	*Herrmann et al*. [2000]
Cl(aq)	1×10^{-13}	*
Cl_2^-(aq)	1×10^{-11}	*Herrmann et al*. [2000]

[#]: gas phase radicals are reported in molecules cm^{-3} and aqueous phase are in M.

*: Calculated from $[Cl_2^-]$, $[Cl^-] = 6.0\times 10^{-4}$ M [*Herrmann, et al.*, 1996], and $K = 1.4\times 10^{5}$ M^{-1} for $Cl + Cl^- \leftrightarrow Cl_2^-$ [*Yu, et al.*, 2004].

Table 6 Summary of sensitivity studies

Conditions	# [MS]	# [NSS]	MS/NSS	Conditions	# [MS]	# [NSS]	MS/NSS
*[BrO] = 10^6	0.26	1.97	0.13	[1]Φ(DMSO) = 0.5	0.67	2.05	0.33
[BrO] = 10^8	5.10	2.99	1.70	[1]Φ(DMSO) = 1.0	0.74	1.99	0.37
*[OH] = 10^5	0.59	1.09	0.55	[2]k'(CH_3S) = 0	0.72	0.25	2.94
[OH] = 10^7	1.75	11.00	0.16	[2]k'(CH_3S) = 10 s^{-1}	0.72	2.06	0.35
*[NO_3] = 10^5	0.72	1.88	0.39	[3]Φ(SO_2) = 0.5	0.72	1.98	0.36
[NO_3] = 10^7	0.71	3.87	0.18	[3]Φ(SO_2) = 1.0	0.72	2.08	0.35
*[Cl] = 10^3	0.73	1.49	0.49	[SO_2] = 0	0.72	2.10	0.35
[Cl] = 10^5	0.69	7.53	0.09	[SO_2] = 60 ppt	0.72	4.80	0.15

* in units of molecules cm^{-3}

steady-state concentrations in units of nmol m^{-3} air

[1] DMSO product yield from DMS + OH

[2] The first order loss rate of CH_3S due to reactions with NO_2, HO_2 and O_3, k'(CH_3S) = 5 s^{-1} for the PS.

[3] SO_2 product yield from CH_3S oxidation, and Φ(SO_2) = 0.8 for the PS.

Table 7 Product yields of SO_2(g), DMSO(g) (pptv) and aqueous phase MS and NSS (pmol m^{-3}) after 15 simulation cycles for scenarios GP, GA, GM, PS and NOS

Species	Scenario				
	GP	GA	GM	PS	NOS
SO_2(g)	40 (64%)	47 (75%)	47 (13%)	5.8 (8%)	8.3 (2%)
DMSO(g)	17 (27%)	3.9 (6%)	95 (27%)	0.2 (0.3%)	104 (27%)
MS	—	—	23 (0.15%)	720 (23%)	25 (0.2%)
NSS	—	—	193 (1.2%)	2100 (67%)	1990 (12%)

Figure Captions

Figure 1. The atmospheric DMS oxidation mechanism used in this study. The dashed lines represent those mechanisms still elusive or unknown. Φ is the product yield and question marks represent reactions with unknown branching ratios or product yields. The reactions in black and blue are abstraction and addition channels of gas phase DMS oxidation, respectively. The reactions and species in red are for aqueous phase transformations, and those reactions in purple arrows represent the heterogeneous processes.

Figure 2. Average liquid water content for (a) 1-hour simulation of the non-drizzling ("ASTEX-1", solid line) and heavily drizzling ("ASTEX-2", dashed line) stratocumulus clouds, and (b) 30-minute simulation of the cumulus cloud (dotted line) considered.

Figure 3. Temporal evolution of in-cloud average (a) MS, (b) NSS and (c) MS/NSS from the simulations of PS when the deposition rates of particles are: 0 (solid lines), 2.0×10^{-6} (dashed lines), 1.0×10^{-5} (dash-dotted lines), 3.0×10^{-5} (star-dotted lines), and 8.0×10^{-5} (dotted lines) in units of s^{-1}.

Figure 4. Vertical profiles of (a) DMSO(g), (b) SO_2(g), (c) MS(aq) and (d) NSS(aq) after 1 (solid), 5 (dashed), 10 (dash-dotted), and 15 (dotted) simulation cycles of PS.

Figure 5. Temporal evolution of (a) MS, (b) NSS and (c) MS/NSS for PS conditions. Five cloud temperatures were considered for simulations of "ASTEX-1" trajectories: 278 K (star-dotted), 288 K (.dotted), 298 K (solid), 308 K (dash-dotted) and 318 K (dashed).

Figure 6. Temporal evolution of (a) MS, (b) NSS and (c) MS/NSS for simulations of "ASTEX-1" (solid), "ASTEX-2" (dashed) and "CF-Cloud" (dotted) trajectories at 300 K.

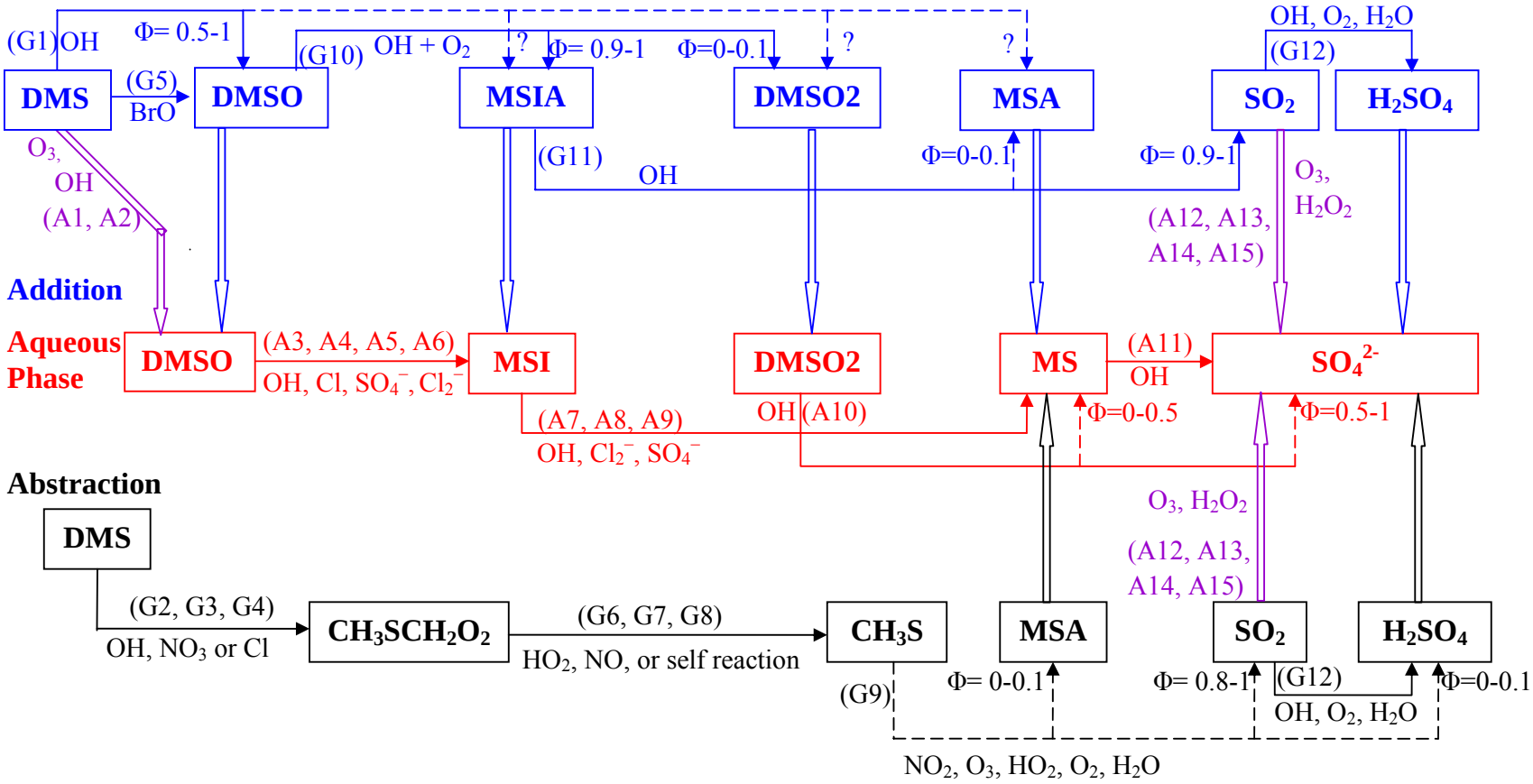
(G1)OH
Φ= 0.5-1
(G10)
OH + O2
?
Φ= 0.9-1
Φ=0-0.1
?
?
OH, O2, H2O
(G12)
DMS
(G5)
BrO
DMSO
MSIA
DMSO2
MSA
SO2
H2SO4
O3,
OH
(A1, A2)
(G11)
OH
Φ=0-0.1
Φ= 0.9-1
O3,
H2O2
(A12, A13,
A14, A15)
Addition
Aqueous
Phase
DMSO
(A3, A4, A5, A6)
OH, Cl, SO4−, Cl2−
MSI
DMSO2
MS
(A11)
OH
SO4 2-
(A7, A8, A9)
OH, Cl2−, SO4−
OH (A10)
Φ=0-0.5
Φ=0.5-1
Abstraction
O3, H2O2
(A12, A13,
A14, A15)
DMS
(G2, G3, G4)
OH, NO3 or Cl
CH3SCH2O2
(G6, G7, G8)
HO2, NO, or self reaction
CH3S
MSA
SO2
H2SO4
(G9)
Φ= 0-0.1
Φ= 0.8-1
(G12)
OH, O2, H2O
Φ=0-0.1
NO2, O3, HO2, O2, H2O

Figure 1

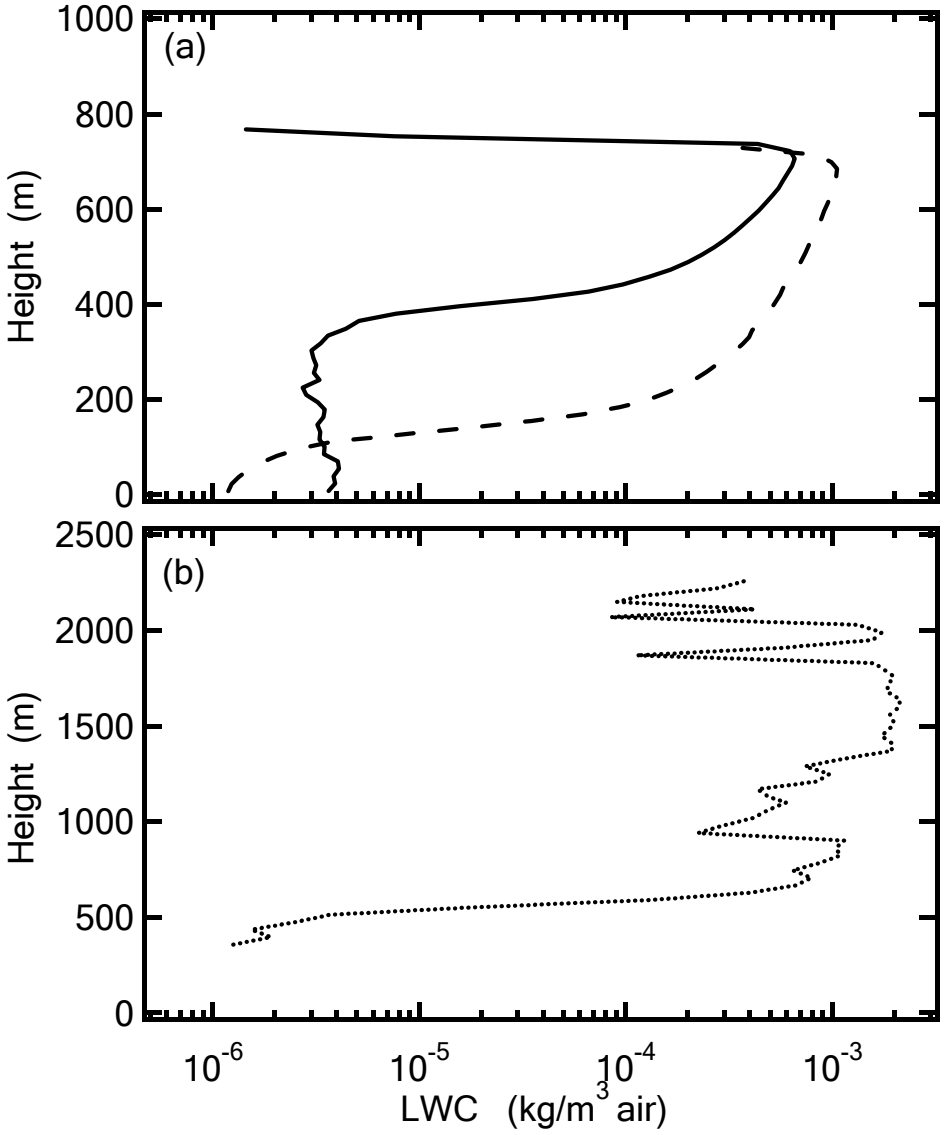
(a)
(b)
Height (m)
Height (m)
1000
800
600
400
200
0
2500
2000
1500
1000
500
0
10^{-6}
10^{-5}
10^{-4}
10^{-3}
LWC (kg/m^3 air)

Figure 2

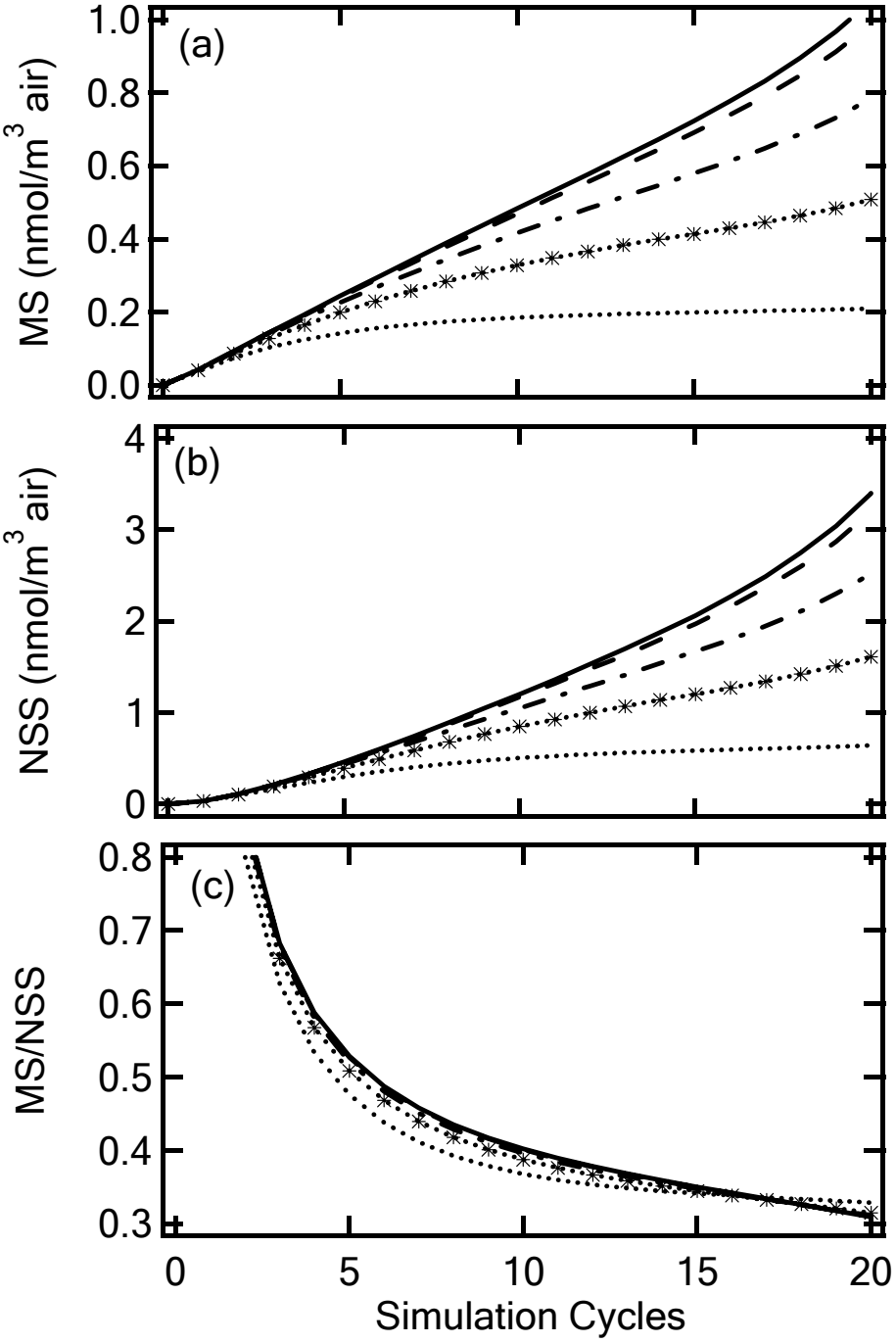
(a)
MS (nmol/m3 air)
1.0
0.8
0.6
0.4
0.2
0.0
(b)
NSS (nmol/m3 air)
4
3
2
1
0
(c)
MS/NSS
0.8
0.7
0.6
0.5
0.4
0.3
0
5
10
15
20
Simulation Cycles

Figure 3

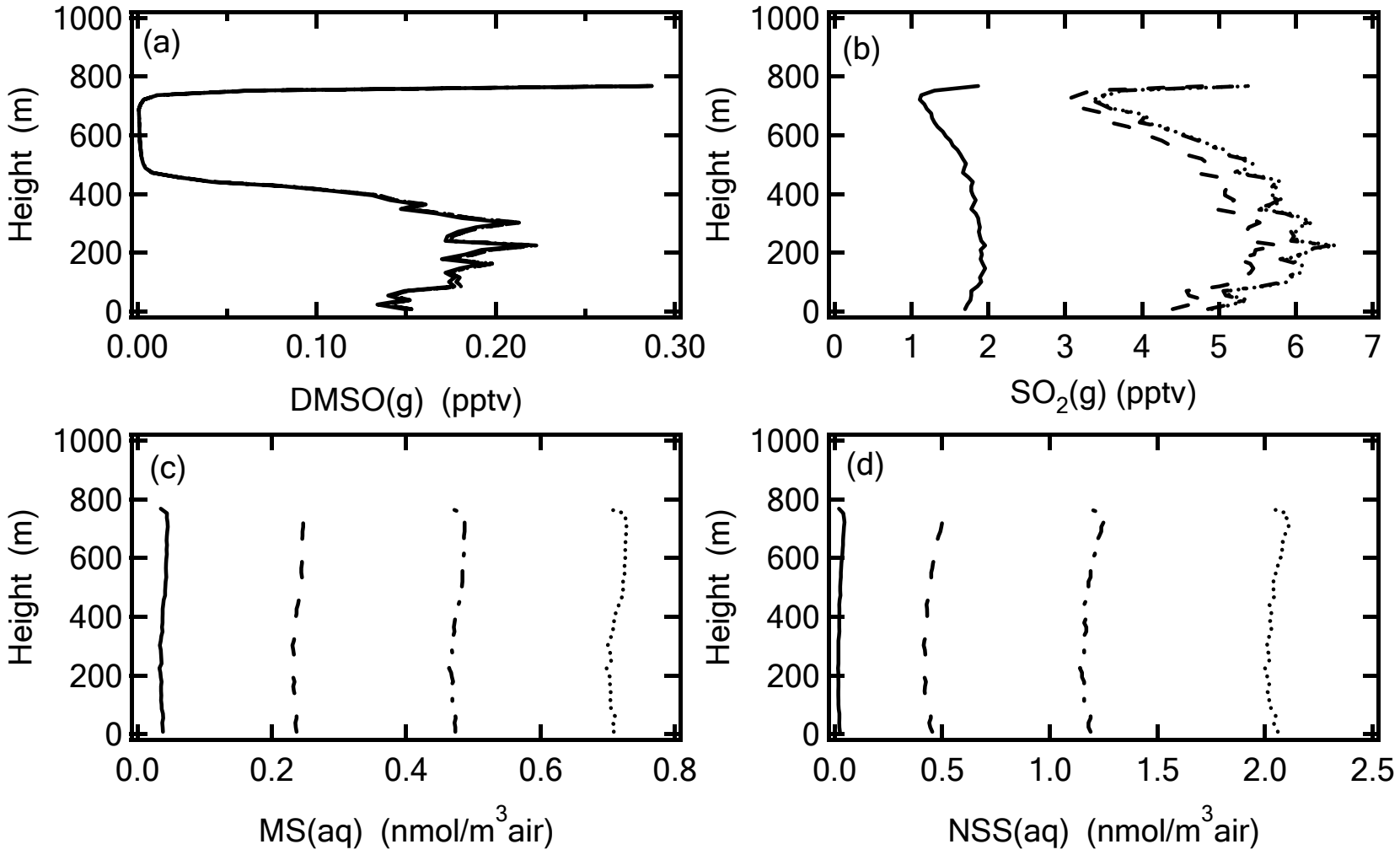
(a)
Height (m)
1000
800
600
400
200
0
0.00
0.10
0.20
0.30
DMSO(g) (pptv)
(b)
Height (m)
0
1
2
3
4
5
6
7
SO2(g) (pptv)
(c)
Height (m)
0.0
0.2
0.4
0.6
0.8
MS(aq) (nmol/m3air)
(d)
Height (m)
0.0
0.5
1.0
1.5
2.0
2.5
NSS(aq) (nmol/m3air)

Figure 4

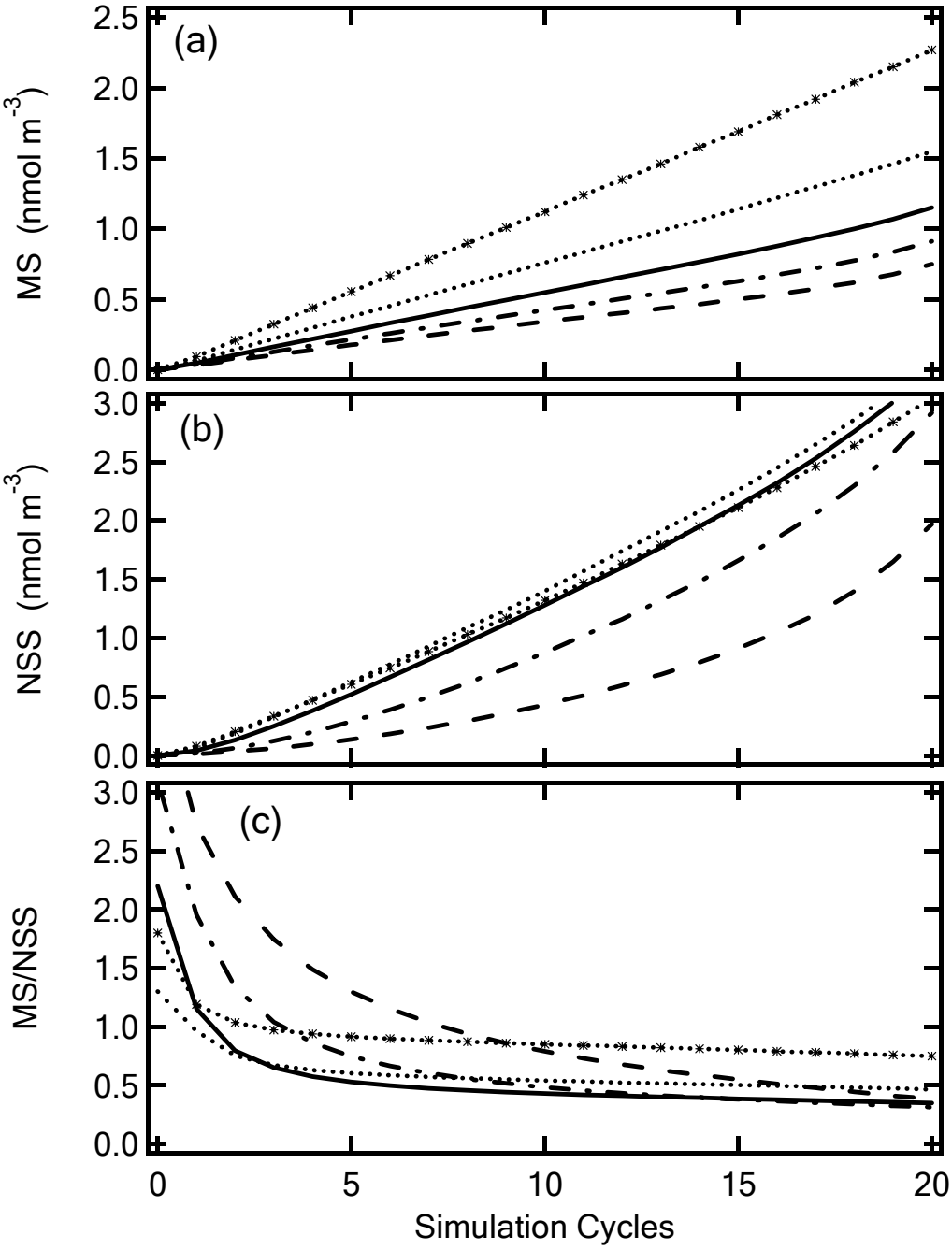
(a)
(b)
(c)
MS (nmol m-3)
NSS (nmol m-3)
MS/NSS
Simulation Cycles
0.0
0.5
1.0
1.5
2.0
2.5
3.0
0
5
10
15
20

Figure 5

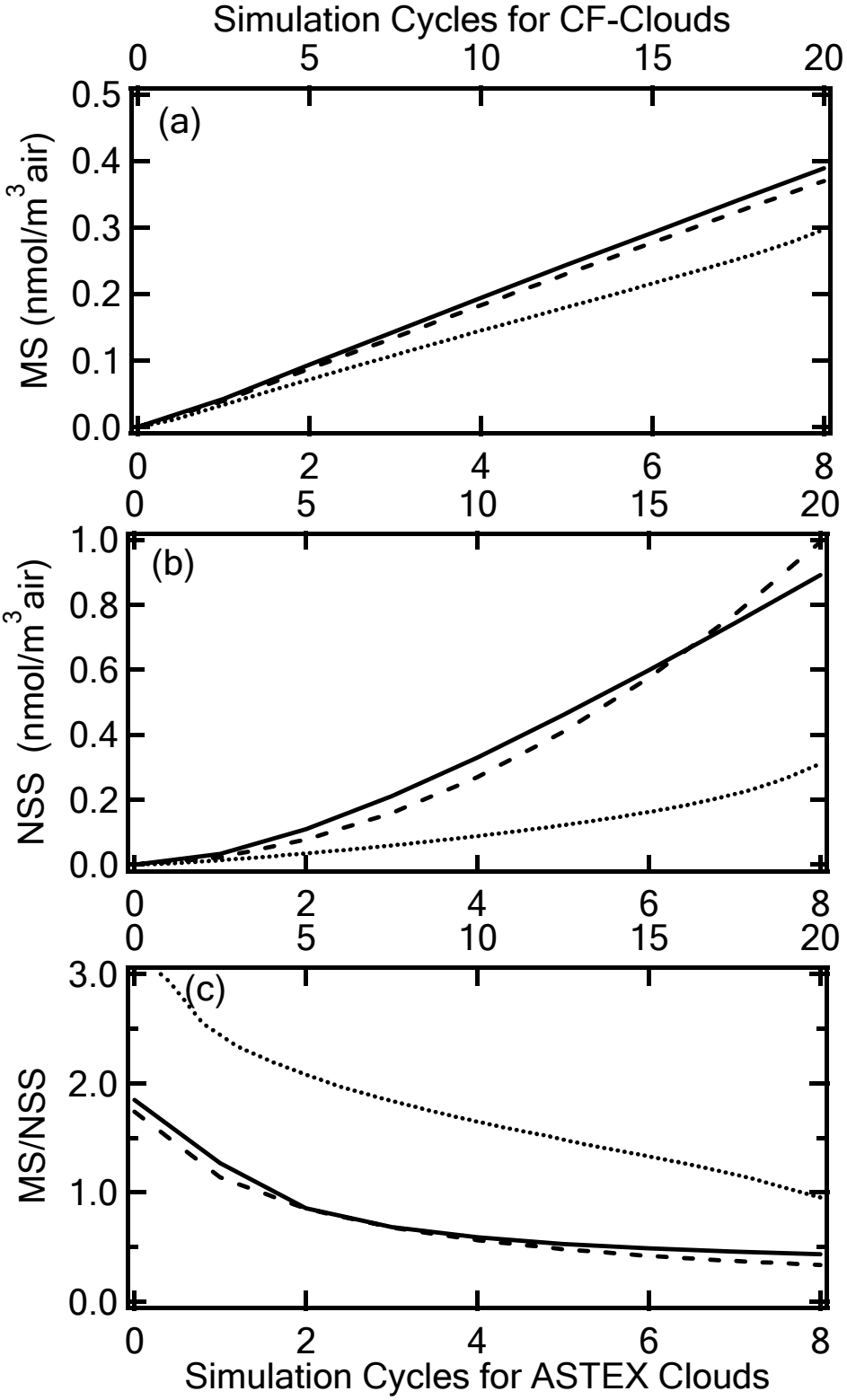
Simulation Cycles for CF-Clouds
0
5
10
15
20
0.5
0.4
0.3
0.2
0.1
0.0
(a)
MS (nmol/m3air)
0
2
4
6
8
0
5
10
15
20
1.0
0.8
0.6
0.4
0.2
0.0
(b)
NSS (nmol/m3air)
0
2
4
6
8
0
5
10
15
20
3.0
2.0
1.0
0.0
(c)
MS/NSS
0
2
4
6
8
Simulation Cycles for ASTEX Clouds

Figure 6